

Implications of the ongoing rock uplift in NW Himalayan interiors

Saptarshi Dey¹, Rasmus Thiede², Arindam Biswas³, Naveen Chauhan⁴, Pritha Chakravarti¹, and Vikrant Jain¹

¹*Earth Science Discipline, IIT Gandhinagar, Gandhinagar-382355, India.*

²*Institute of Geosciences, Christian Albrechts University of Kiel, Kiel-24118, Germany.*

³*Department of Applied Geology, IIT-ISM Dhanbad, Jharkhand-826004, India.*

⁴*Atomic Molecular and Optical Physics Division, Physical Research Laboratory, Ahmedabad.*

Corresponding author

Saptarshi Dey

saptarshi.dey@iitgn.ac.in

Abstract

The Lesser Himalaya exposed in the Kishtwar Window (KW) of the Kashmir Himalaya exhibits rapid rock uplift and exhumation (~3 mm/yr) at least since the Late Miocene. However, it has remained unclear if it is still actively-deforming. Here, we combine new field observations, morphometric and structural analyses with dating of geomorphic markers to discuss the spatial pattern of deformation across the window. We found two steep stream segments, one at the core and the other along the western margin of the KW, which strongly suggest ongoing differential uplift and may possibly be linked either to crustal ramps on the MHT or active surface-breaking faults. High bedrock incision rates (> 3 mm/yr) on Holocene/Pleistocene timescales are deduced from dated strath terraces along deeply-incised Chenab River valley. In contrast, farther

downstream on the hanging wall of the MCT, fluvial bedrock incision rates are lower (< 0.8 mm/yr) and are in the range of long-term exhumation rates. Bedrock incision rates largely correlate with previously-published thermochronologic data. In summary, our study highlights a structural and tectonic control on landscape evolution over millennial timescales.

Keywords

Steepness index; knickzone, rock strength; bedrock incision; Main Himalayan Thrust.

1. Introduction

Protracted convergence between the Indian and the Eurasian plate resulted into the growth and evolution of the Himalayan orogen and temporal in-sequence formation of the Southern Tibetan Detachment System (STDS), the Main Central Thrust (MCT), the Main Boundary Thrust (MBT) and the Himalayan Frontal Thrust (HFT) towards the south (e.g., Yin and Harrison, 2000; DiPietro and Pogue, 2004) (Supplementary Fig.B1). HFT defines the southern termination of the Himalayan orogenic wedge and separates the orogen from the undeformed foreland basin known as the Indo-Gangetic Plains. Seismic reflection profiles reveal that all these fault-zones emerge from a low-angle basal decollement, the Main Himalayan Thrust (MHT) forming the base of the Himalayan orogenic wedge (e.g., Ni and Barazangi, 1984; Nabelek et al., 2009; Avouac et al., 2016), established in the late Miocene (Vannay et al., 2004). Existence of MHT has further been elaborated in Himalayan cross-sections (e.g., Powers et al., 1998; Decelles et al., 2001; Webb et al., 2011; Gavillot et al., 2018).

Lave and Avouac (2000) studied the late Pleistocene-Holocene shortening history of the Central Nepal Himalaya where they showed the Holocene shortening is accommodated only across the HFT. However, a large body of literature in the eastern, central and western Himalaya favored that majority of the late Pleistocene-Holocene shortening is rather partitioned throughout the Sub-Himalayan domain (morphotectonic segment in between the MBT and the MFT) and not solely accommodated by the HFT (e.g., Wesnousky et al., 1999; Burgess et al., 2012; Thakur et al., 2014; Mukherjee, 2015; Vassalo et al., 2015; Dey et al., 2016; Dey et al., 2018). The statement above implies that the northerly thrusts, i.e., the MBT and the brittle faults exposed in the vicinity of the southern margin of the Higher Himalaya, are considered inactive over millennial timescales. However, in recent years, several studies which focused on the low-temperature thermochronologic data and thermal modeling of the interiors of the NW Himalaya have raised questions on the statement above. The recent studies suggested that 1-3 mm/yr out of the total Quaternary shortening has been accommodated in the north of the MBT as out-of-sequence deformation (Thiede et al., 2004; Deeken et al., 2011; Thiede et al., 2017) or in form of growth of the Lesser Himalayan Duplex (Gavillot et al., 2018) (Supplementary Fig. B2). For faults within the hinterland of the Central Himalaya, the out-of-sequence deformation has been explained by two end-member models. One of them favored the reactivation of the MCT (Wobus et al., 2003), while the other tried to explain all changes along the southern margin of the Higher Himalaya driven by enhanced rock uplift over a major ramp on the MHT (Bollinger et al., 2006; Herman et al., 2010; Robert et al., 2009). Landscape evolution models, structural analysis and thermochronologic data from the interior of the Himalaya favor that the Lesser Himalaya has formed a duplex at the base of the southern Himalayan front by sustained internal deformation since late Miocene (Decelles et al., 2001; Mitra et al., 2010; Robinson and Martin, 2014; Gavillot

et al., 2016). The growth of the duplex resulted ~~into~~ the uplift of the Higher Himalaya forming the major orographic barrier of the orogen. The Kishtwar Window (KW) in the NW Himalaya represents the northwestern termination of the Lesser Himalayan Duplex (LHD). While most of the published cross-sections of the Himalayan orogen today recognize the duplex structures within the Lesser Himalaya (Webb et al., 2011; Mitra et al., 2010; DeCelles et al., 2001; Gavillot et al., 2018), little or no data are available on how the deformation is spatially as well as temporally distributed and most importantly, whether a duplex is active over millennial timescales.

The low-temperature thermochron study by Kumar et al., (1995) portrayed the first orogen-perpendicular sampling traverse extending from the Kishtwar tectonic Window over the Zaskar Range. More recent studies link the evolution of the KW to the growth of the Lesser Himalayan Duplex structure (Gavillot et al., 2018), surrounded by the Miocene MCT shear zone along the base of the High Himalayan Crystalline, locally named as the Kishtwar Thrust (KT) (Ul Haq et al., 2019). Thermochronological constraints suggest higher rates of exhumation within the window (3.2-3.6 mm/yr) with respect to the surroundings (~0.2 mm/yr) (Gavillot et al., 2018), corroborating ~~well with~~ similar thermochron-based findings from the of the Kullu-Rampur window along the Beas (Stübner et al., 2018) and Sutlej valley (Jain et al., 2000; Vannay et al., 2004; Thiede et al., 2004) over ~~the~~ Quaternary timescale. No evidence exists whether the hinterland of the Kashmir Himalaya is tectonically-active over intermediate timescales. Therefore, to understand the 10^3 - 10^4 -year timescale neotectonic evolution, we combined geological field evidences, chronologically-constrained geomorphic markers and morphometric analysis of ~~potential study areas, such as~~ the KW. The detailed structural information of the window and ~~the~~ surroundings, previously-published thermochron data,

accessibility, well-preserved sediment archive, and recognizable geomorphic markers across the Kishtwar Window makes it a ~~potent~~ location for our study.

In this study, we focus on the following long-standing questions on Himalayan neotectonic evolution, which are-

1. Is there any ongoing neotectonic deformation in the interiors of the Kashmir Himalaya?

2. Can we determine sub-surface structural variations and existence of surface-breaking faults by analyzing terrain morphology?

3. Can we obtain new constraints on deformation over geomorphic timescales? Do millennial-scale fluvial incision rates support long-term exhumation rates?

To address these questions, we adopted a combination of methods ~~such as~~ morphometric analysis using high-resolution digital elevation models, field observation on rock type, structural variations as well as rock strength data and, analysis of satellite images to assess the spatial distribution of the late Quaternary deformation of the KW and surroundings (Fig.1). We aimed to evaluate the role of active tectonics and geometric variations in the basal decollement in shaping the topography (Fig.1). We used basinwide steepness indices and specific stream power as a proxy of fluvial incision. And, lastly but most importantly, we calculated the fluvial bedrock incision rates by using depositional ages of aggraded sediments along Chenab River. In this study, we show that the regional distribution of topographic growth is concentrated in the core of the window and along the western margin of the window. Our new estimates ~~on the~~ bedrock incision rate agree with Quaternary exhumation rates from the KW, which could mean consistent active growth of the Kishtwar Window over million-year to millennial timescales. Although the

observed topographic and morphometric pattern indicate a structural/tectonic control on topographic evolution, with the available data we are not able to resolve whether it is caused by passive translation on the MHT or by active surface-breaking faulting within the duplex.

2. Geological background

Regionally balanced cross-sections (DiPietro and Pogue, 2004; Searle et al., 2007; Gavillot et al., 2018) suggest that the Himalayan wedge is bounded at the base by décollement, named the MHT, and all regionally-extensive surface-breaking thrust systems are rooted to it. The orogenic growth of the Himalaya resulted into an overall in-sequence development of the orogen-scale fault systems which broadly define the morphotectonic sectors of the orogen (Fig. 1b). Notable among those sectors, the Higher Himalaya is bordered by the MCT in the south and is comprised of high-grade metasediments, Higher Himalayan Crystalline Sequence (HHCS) and Ordovician granite intrusives (Fuchs, 1981; Steck, 2003; DiPietro and Pogue, 2004; Gavillot et al., 2018). The Low-grade metasediments (quartzites, phyllites, schists, slates) of the Proterozoic Lesser Himalayan sequence are exposed between the MCT in the north and MBT in the south. The Lesser Himalayan domain is narrow (4-15 km) in the NW Himalaya except where it is exposed in the form of tectonic windows (Kishtwar window, Kullu-Rampur window etc.) in the western Himalaya (Steck, 2003). The Sub-Himalayan fold-and-thrust belt lying to the south of the MBT is tectonically the most active sector since the late Quaternary (Gavillot, 2014; Vassallo et al., 2015; Gavillot et al., 2018).

Near the southwest corner of our study area, Proterozoic low-grade Lesser Himalayan metasediments are thrust over the Tertiary Sub-Himalayan sediments along the MBT (Wadia,

1934; Thakur, 1992). Near the Chenab region in the Kashmir Himalaya, Apatite U-Th/He ages suggest that cooling and exhumation related to faulting along the MBT thrust sheet initiated before $\sim 5 \pm 3$ Myr (Gavillot et al., 2018). Geomorphic data obtained across the MBT in Kashmir Himalaya suggest that MBT has not been reactivated for the last 14-17 kyr (Vassallo et al., 2015). In the Kashmir Himalaya, the Lesser Himalayan sequence (LHS) exposed between the MBT and the MCT is characterized by a < 10 km-wide zone of sheared schists, slates, quartzites, phyllites and Proterozoic intrusive granite bodies (Bhatia and Bhatia, 1973; Thakur, 1992; Steck, 2003). The LHS is bounded by the MCT shear zone in the hanging wall. The MCT hanging wall forms highly deformed nappe exposing lower and higher Haimantas, which are related to the Higher Himalayan Crystalline Sequence (HHCS) (Bhatia and Bhatia, 1973; Thakur, 1992; Yin and Harrison, 2000; Searle et al., 2007; Gavillot et al., 2018). Nearly 40 km NE of the frontal MCT shear zone, ~~MCT fault zone~~ is re-exposed as a klippe in the vicinity of KW is called the Kishtwar Thrust (KT) (Ul Haq et al., 2019) (fig. 1). Within the KW, Lesser Himalayan quartzites, low-grade mica schists and phyllites along with the granite intrusives are exposed (Fuchs, 1975; Steck, 2003; DiPietro and Pogue, 2004; Yin, 2006; Gavillot et al., 2018).

2.1. Structural architecture of the Kishtwar Window

The sub-surface structural formation beneath the KW is not well-constrained. A recent study by Gavillot et al., (2018) proposes that the KW exposes a stack of LHS nappes in form of the commonly-known Lesser Himalayan Duplex (LH duplex), characteristic of the central Himalaya (Decelles et al., 2001). They also propose the existence of two mid-crustal ramps beneath the KW, viz., MCR-1 and MCR-2 (fig. 1b). Based on thermochronological constraints from Kumar et al., (1995), Gavillot et al. (2018) proposed that the core of the window ~~is exhumed with~~ rates $3.2-3.6$ mm/yr during the Quaternary, at a higher rate when compared to the

surroundings (~0.2-0.4 mm/yr). However, earlier studies by Fuchs (1975) and Frank et al.; (1995) provide different insights to the formation of the KW. Fuchs (1975) proposed the existence of two nappes- a. the Chail Nappe and b. the Lower Crystalline Nappe. The Lower Crystalline nappe is partially or completely included in the MCT (KT) shear zone and the Chail nappe encompasses the core of the window (Stephenson et al., 2000). According to these studies, the Chail nappe has been internally deformed by crustal buckling, tight isoclinal folding causing repetition and thickening of the LH crust.

The Higher Himalayan sequence dips steeply away from the duplex (~65° towards west) (Fig.1, 2a). The frontal horses of the LH duplex expose internally-folded greenschist facies rocks. Although at the western margin of the duplex, the quartzites stand sub-vertically (Fig.2c), the general dip amount reduces as we move from west to east for the next ~10-15 km up to the core of the KW. Near the core of the KW, we observed highly-deformed (folded and multiply-fractured) quartzite at the core of the KW (Fig.2d, 2e). We also observed deformed quartz veins of at least two generations, as well as macroscopic white mica. Here, the Chenab River is also very steep and narrow; the rock units are also steeply-dipping towards the east (~55-65°) and are nearly isoclinal and strongly deformed at places (Fig.2f). Towards the eastern edge of the window, however, the quartzites dip much gently towards the east (~20-30°) (Fig.1b), and much lesser folding and faulting have been recognized in the field (Fig.2g).

2.2.Valley morphology

The broad, 'U-shaped' valley profile near the town of Padder at the eastern margin of the KW is in contrast with the interior of the window (Fig.3a). At the core of the KW, the Chenab River maintains a narrow channel width and a steep gradient (Fig.3b). The E-W traverse of the Chenab River through the KW is devoid of any significant sediment storage. However, along the

179 N-S traverse parallel to the western margin of the KW, beneath the Kishtwar surface, ~150-170m
180 thick sedimentary deposits are transiently-stored over the steeply-dipping Higher Himalayan
181 bedrock (Fig.3c). The height of the Kishtwar surface from the Chenab River is ~450m, which
182 means ~280m of bedrock incision by the River since the formation of the Kishtwar surface.
183 Along the N-S traverse of the River, epigenetic gorges are formed as a result of the damming of
184 paleo-channel by the hillslope debris flow, followed by the establishment of a newer channel
185 path (Ouimet et al., 2008; Kothyari and Juyal, 2013). One example of such epigenetic gorge
186 formation near the town of Drabshalla is shown in Fig.3d. Downstream from the town of
187 Drabshalla, the River maintains narrow channel width (< 25 m) and flows through a gorge
188 having sub-vertical valley-walls (Fig.3e). The tributaries originating from the Higher Himalayan
189 domain form one major knickpoint close to the confluence with the trunk stream (Fig.3f). We
190 have identified at least three strath surface levels above the present-day river channel, viz., T1
191 (280 ± 5 m), T2 (170-175 m) and T3 ($\sim 120 \pm 5$ m), respectively (Fig.3g). The first study on
192 sediment aggradation in the middle Chenab valley (transect from Kishtwar to Doda town) was
193 published by Norin (1926). He argued the sediment aggradation in and around the Kishtwar town
194 is largely contributed by fluvioglacial sediments and the U-shaped valley morphology is a
195 marker of past glacial occupancy. In general, we agree with the findings of Norin (1926) and Ul
196 Haq et al., (2019) as we observe ~100m thick late Pleistocene fluvioglacial sediment cover
197 unconformably overlying the Higher Himalayan bedrock, most likely to be paleo-strath surface
198 (Fig.4b). At the same time, we do not agree with the interpretation of surface-breaking faults
199 near Kishtwar town by Ul Haq et al. (2019). We inspected the proposed fault locations in detail
200 and didn't observe any evidence of large-scale fault movement, including offset, broken and
201 rotated clasts, fault gouges etc. on the proposed fault planes. There is only one ~~evidence of a~~

deformed sand layer which shows tilting and offset (<1 m). Therefore, we ~~may~~ conclude that we found no strong evidence of any large-scale surface-breaking faults. The fluvioglacial sediments included alternate layers of pebble conglomerate and coarse-medium sand (Fig.4c). The pebbles are moderately rounded and polished suggesting significant fluvial transport. Our field observations suggest that the fluvioglacial sediments have been succeeded by a significant volume of hillslope debris flow and paleo-landslide deposit (Fig.4c). The thickness of the debris-flow deposits is variable. The hillslope debris units and landslide deposits contain mostly massive, highly-angular, poorly-sorted quartzite clasts from the steep western margin of the KW. The hillslope debris units also contain a few fine-grain sediment layers trapped in between two coarse-grained debris layers (Fig.4e). The town of Kishtwar is situated on this debris flow deposit.

3. Methods of morphometric analysis and field data collection

3.1.Morphometry

For conducting the morphometric analysis, we have used 12.5m ALOS-PALSAR DEM data (high resolution terrain-corrected) (Fig.5a). This DEM data has lesser issues with artifacts and noises than 30m SRTM data, which fails to capture the drainage network properly in areas populated by narrow channel gorges. Topographic relief has been calculated using a 4km moving window (Fig.5b) and the rainfall distribution pattern has been adapted from 12-year averaged annual rainfall data (TRMM data: Bookhagen and Burbank, 2006) (Fig.5c).

3.1.1. Drainage network extraction

The drainage network and the longitudinal stream profiles were extracted using the Topographic Analysis Kit toolbox (Forte and Whipple, 2019). An equivalent of 10-pixel smoothing of the raw DEM data has been applied to remove noises from the DEM. The longitudinal stream profile of the Chenab trunk stream was processed with the Topotoolbox ‘Knickpointfinder’ tool (Schwanghart and Scherler, 2014). Several jumps/ kinks in the longitudinal profile are seen and those are marked as knickpoints (Fig.6). A 30m tolerance threshold was applied to extract only the major knickpoints.

3.1.2. Basinwide normalized steepness indices

Global observations across a broad spectrum of tectonic and climatic regimes have revealed a power-law scaling between the local river gradient and upstream contributing area:

$$S = k_s \cdot A^{-\theta} \quad (1)$$

where S is the stream gradient (m/m), k_s is the steepness index ($m^{2\theta}$), A is the upstream drainage area (m^2), and θ is the concavity index (Flint, 1974; Whipple and Tucker, 1999). Normalized steepness-index values (k_{sn}) are steepness indices calculated using a reference concavity value (θ_{ref}), which is useful to compare steepness-indices of different river systems (Wobus et al., 2006). We extracted the k_{sn} values in the study area using the ArcGIS and MATLAB-supported Topographic Analysis Toolkit (Forte and Whipple, 2019) following the procedure of Wobus et al. (2006). We performed an automated k_{sn} extraction using a critical area of $10^6 m^2$ for assigning the channel head, a smoothing window of 500 m, a θ_{ref} of 0.45, and an auto- k_{sn} window of 250 m for calculating k_{sn} values. The slope-breaks, known as the knickpoints (sometimes referred to as knickzones if it is manifested by a series of rapids instead of a single sharp break in profile), were allocated by comparing the change of slope along the distance-elevation plot (Fig.6, 7a). Threshold ‘dz’ value (projected stream offset across a knickpoint) for

this study is 30m. Basinwide mean k_{sn} values are plotted using a 1000 km² threshold catchment area (Fig. 5d).

Identification of the knickpoints/ knickzones and their relationship with the rock-types as well as with existing structures are necessary to understand the causal mechanism of the respective knickpoints/ knickzones. Knickpoints/(zones) can be generated by lithological, tectonic and structural control. Lithological knickpoints are stationary and anchored at the transition from the soft-to-hard substrate. The tectonic knickpoints originate at the active tectonic boundary and migrate upstream with time. Structural variations, such as thrust fault ramp-flat geometry, may cause a quasistatic knickpoint at the transition of the flat-to-ramp of the fault. In such cases, the ramp segment is characterized by higher steepness than the flat segment and at times the ramp may be characterized by a sequence of rapids, forming a wide knickzone, instead of a single knickpoint.

3.1.3. Channel Width

Channel width is a parameter of assessment of lateral erosion/incision through bedrocks of equivalent strength (Turowski, 2009). The channel width of the Chenab trunk stream from just downstream of the MBT up to the eastern margin of the KW was derived by manual selection and digitization of the channel banks using the Google Earth Digital Globe imagery (<http://www.digitalglobe.com/>) of minimum 3.2 m spatial resolution. We used the shortest distance between the two banks as the channel width. We rejected areas having unparallel channel-banks as that would bias the result. We used a 50 m step between two consecutive points for channel width determination. Twenty point-averaged channel width data along with elevation of the riverbed is shown in Fig.7b.

3.1.4. Specific stream power (SSP) calculation

Specific stream power has often been used as a proxy of fluvial incision or differential uplift along the channel (Royden and Perron, 2013; Whipple and Tucker, 1999). Areas of higher uplift/incision are characterized by transient increase in the specific stream power. Channel slope and channel width data were used to analyse the corresponding changes in the specific stream power (SSP) from upstream of the gorge area to the gorge reaches (Bagnold, 1966). The SSP (ω) was estimated using the following equation –

$$\omega = \gamma \cdot Q \cdot s / w \quad (\text{Eq. 1})$$

Where, γ - unit weight of water, Q – water discharge, s – energy slope considered equivalent to the channel slope; w – channel width. SSP data from selected stretches are shown in Table 1. Channel width has been adapted from method described in section 3.1.3. We assumed a uniform discharge throughout the study area, as the TRMM data show insignificant variations in mean annual rainfall (Bookhagen and Burbank, 2006) (Fig. 5c, 5e). We also assume a runoff ratio of 1 as we ~~don't have~~ any independent measure or supportive data of runoff vs. water percolation through the bedrock and sediment archive.

3.2. Field data collection

3.2.1. Structural data

We measured the strike and dip of the foliations and bedding planes of the Lesser and Higher Himalayan rocks using the Freiberg clinometer compass. At least five measurements are taken at every location and the average of them has been reported in Fig. 8a. Field photos in the Fig.2 support observed variations in the structural styles.

3.2.2. Rock strength data

Recording rock strength data in the field is important to understand the role of variable rock-type and rock-strength in changes in morphology. It provides us important insights on the genesis of knickpoints whether they are lithologically-controlled or not. It also helps to understand the variations in channel steepness across rocks of similar lithological strength. We systematically measured the rock strength of the main geologic units using a hand-held rebound hammer. Repeated measurements (8-10 measurements at each of the 75 locations throughout the study area) were conducted to measure the variability of rock-strength within the main lithologic units (Fig. 7e). All the measurements were taken perpendicular to the bedding/ foliation plane, and, no measurements are from wet surfaces or surfaces showing fractures. Each reading was taken at least 0.5m apart from the previous one. To our benefit, most of the road-cut sections had bedrock-exposures. Except restricted locations, e.g., dam-sites and military bases and outposts, we were able to cover rest of the study area. ~~To add to this,~~ data taken from Higher Himalayan intrusives close to the western margin of the KT are positively-biased as it represents readings only from the leucosomatic layers. Our data from individual sites are smaller in number than what is preferred for checking the statistical robustness of Schmidt hammer data (Niedzielski et al., 2009). Therefore, we combined the data from all sites representing similar lithology and portrayed the mean \pm standard deviation for ~~the same~~. Field data on rock strength measurement ~~has~~ been provided in Supplementary Table C1.

3.3. Luminescence dating of transiently-stored sediments in and around Kishtwar

Luminescence dating of Quaternary sediments is a globally accepted method for constraining the timing of deposition of sediments across different depositional environments, viz., Aeolian (Juyal et al., 2010), fluvial (Olley et al., 1998; Cunningham and Wallinga, 2012) and glacial origin (Owen et al., 2002; Pant et al., 2006). In this study, we used luminescence

315 dating ~~techniques~~ to constrain depositional ages of several fluvioglacial and fluvial sand layers
316 exposed near the western margin of the KW and further downstream. Although there exists a few
317 persistent problems in luminescence dating of the Himalayan sediments (including poor
318 sensitivity of quartz and numerous cases of heterogeneous bleaching of the luminescence signal),
319 studies over the past couple of decades have also provided a good control on Himalayan
320 sedimentary chronology by using luminescence dating with quartz (Optically stimulated
321 luminescence, OSL) and feldspar (Infra-red stimulated luminescence, IRSL).

322 Samples K-07, K-08 and K-09 were collected from the medium-coarse sand beds of
323 fluvioglacial origin and have been dated with IRSL technique (Preusser, 2003). Standard IR-
324 protocol was used because the OSL signal was saturated and postIR-IR was showing instances of
325 heterogeneous bleaching. Samples K-02 and K-11 were taken from the fine sand-silt layers lying
326 above the debris-flow deposits and have been treated for OSL dating using double-SAR (single
327 aliquot regenerative) protocol (Roberts, 2007). Double-SAR protocol was used to surpass the
328 luminescence signal from tiny feldspar inclusions within individual quartz grains. Samples K-16
329 and K-17 taken above the T3 strath level, as well as the sample K-18, taken from above the T1
330 strath level were treated/ measured following the OSL double-SAR protocol. Samples K-01 and
331 K-06 taken above the bedrock strath near the town of Doda were also measured following OSL
332 double-SAR protocol. The aliquots were considered for equivalent dose (ED) estimation only if:
333 (i) recycling ratio was within 1 ± 0.1 , (ii) ED error was less than 20%, (iii) test dose error was less
334 than 10%, and (iv) recuperation was below 5% of the natural. Fading correction of the IRSL
335 samples K-07 and K-09 were done using conventional ~~fading correction~~ method (Huntley and
336 Lamothe, 2001). For samples showing over-dispersion (OD) $\leq 20\%$, central age model (CAM)
337 ~~has been~~ used for estimation of equivalent dose (D_e) (Bailey and Arnold, 2006) instead of

RMM-based De estimation as prescribed by Chauhan and Singhvi, (2011), useful for samples having higher over dispersion (Table 2). For samples K-16 and K-17 having high OD value, minimum age model (MAM) ~~has been~~ used. Details of sample preparation are provided in supplement.

The dose rate was estimated using online software DRAC (Durcan et al., 2015) from the data of Uranium (U), Thorium (Th) and Potassium (K) measured using ICP-MS and XRF (Table 2) in IISER Kolkata. The estimation of moisture content was done by using the fractional difference of saturated vs. unsaturated sample weight (Table 2).

4. Results

4.1. Field observations and measurements

The Chenab River has deeply incised the KW (Fig. 3b and 3e). The LHS rock units exposed within the KW are mainly composed of fine-grain Quartzites and phyllites with occasional schists in between (Steck, 2003; Gavillot et al., 2018). The Lesser Himalaya has been suggested to be an asymmetric antiformal stack with a steeper western flank (dip: 70°/west) (Fig.2c). The KW is surrounded by rock units related to the Higher Himalayan high-grade metasedimentary sequence, mainly garnet-bearing mica schists and gneisses. Higher Himalayan rocks close to the western edge of the KW form a klippe with a southwest-verging MCT at its² base. The KT, southern structural boundary of the window margin accommodating the differential exhumation between window internal and surroundings, is expressed as highly deformed sub-vertical shear bands.

Along the traverse of the Chenab River through the KW and further downstream, two prominent stretches along the Chenab River ~20 and ~25-30 km length are characterized by

steep channel gradient associated with a large number of rapids (Fig.3b). These steep segments are also characterized by a very narrow channel width ($< 30\text{m}$) (Fig.3b, 3e). The steepened segments define knickzone (KZ) rather than a single knickpoint (KP). The knickzones KZ1 in the trunk stream as well as in the tributaries are hosted over bedrock gorges. Although the knickzone KZ2 pass through a series of old landslides (around Kishtwar town), the rapids have all formed in bedrock channel. Therefore, neither KZ1 nor KZ2 appears to be related to damming by recent landslides or other mass movements. The eastern margin of the KW is characterized by a wide 'U-shaped' valley filled with thick sand layers and coarser fluvio-glacial sediments (Fig. 3a) where the Chenab River incises through this Late Pleistocene fill at present.

The rock strength data taken along the Chenab trunk stream portray large variations (R-value ranging from 28 to 62) across different morphotectonic segments (Fig.7e). Within the KW, Lesser Himalayan phyllites and schists have low R values (30-35); however, the low-strength schists and phyllites are sparsely present and therefore, they are ignored while plotting the regional rock strength values in Fig.7e. The dominant Lesser Himalayan quartzites in KW, as well as the granitic intrusives in the eastern part of the KW, shows very high R values of 55-62 and 51-56 respectively (Fig. 7e). Compared to the high R values in the KW, the Higher Himalayan metasediments show low strength (R: 35-45) till the point KP5 (Fig. 3b). However, near the western margin of the KW, the migmatites of Higher Himalayan domain show high rock strength (R value: 58 ± 3) (Fig.7e). The rock strength increases within the Haimanta Formation (R: 44 ± 2) further downstream until it reaches the MCT shear zone at the southern boundary of the Main Himalayan orogen. The R-value in the frontal Lesser Himalaya is moderate (R: 41 ± 2).

The Higher Himalayan sequence dips steeply away from the duplex ($\sim 65^\circ$ towards west) (Fig.2a, 8a). The frontal nappes of the Lesser Himalaya expose internally-folded greenschist

facies rocks. Although at the western margin of the duplex, the quartzites stand sub-vertically, the general dip amount reduces as we move from west to east for the next ~10-15 km (Fig. 8). Near the core of the KW, we observed deformed quartz veins of at least two generations, as well as macroscopic white mica. Near the core of the window, where the river is also very steep and narrow, the rock units are also steeply-dipping towards the east (~60-65°) and are ~~extremely~~ nearly isoclinal and vigorously deformed at places (Fig.2d, 2e). Towards the eastern edge of the window, however, the quartzites dip much gently towards the east (~25-30°) and much lesser folding and faulting have been recognized in the field.

The E-W traverse of the Chenab River is completely devoid of any sediment storage. However, along the N-S traverse parallel to the western margin of the KW, ~150-170m thick sedimentary deposits are transiently-stored over the steeply-dipping Higher Himalayan bedrock. Norin (1926) argued the sediment aggradation in and around the Kishtwar town is largely contributed by fluvioglacial sediments and the U-shaped valley morphology is a marker of past glacial occupancy. We partially agree to the findings of Norin (1926) and Ul Haq et al., (2019) as we observe >100m thick fluvioglacial sediment cover unconformably overlying the Higher Himalayan bedrock along the N-S traverse of the Chenab River. The fluvioglacial sediments included alternate layers of pebble conglomerate and coarse-medium sand. The pebbles are moderately rounded and polished suggesting significant fluvial transport. Our field observations suggest that the fluvioglacial sediments have been succeeded by a significant volume of hillslope debris. The thickness of the debris-flow deposits is variable. The hillslope debris units contain mostly coarse-grained, highly-angular, poorly-sorted quartzite clasts from the frontal horses of the Lesser Himalayan Duplex. The town of Kishtwar is situated on this debris flow deposit (Fig.9). Along the N-S traverse of the Chenab, we have observed at least two epigenetic gorges

lying along the main channel (Fig. 3d). The active channel has incised the Higher Himalayan bedrock and formed strath surfaces. We have identified at least three strath surface levels above the present-day river channel, viz., T1 (280 ± 5 m), T2 (170-175 m) and T3 ($\sim 120\pm 5$ m), respectively (Fig.3g, 10a).

4.2. Results from morphometric analysis

4.2.1. Steep stream segments and associated knickpoints

The longitudinal stream profile along the Chenab River does not portray a typical adjusted concave-up profile across the Himalaya (Fig. 6). We observe breaks in slope and concavity at several locations within a ~ 150 km traverse upstream from the MBT across the KW. These breaks are defined as knickpoints. Starting from the eastern margin of the KW till the MBT in the downstream, we identified at least six (6) discrete knickpoints in the river profile (Fig. 6). Those are named KP1–KP6 according to their decreasing elevations. The upstream head of KZ1 and KZ2 are marked as KP2 and KP3, respectively (Fig. 6). The slope breaks define the upstream reaches of the steep stream segments. The basinwide steepness indices span from ~ 30 – $>750 \text{ m}^{0.9}$ across the study area (Fig. 5d). We assigned a threshold value of $k_{sn} > 550$ for the steepest watersheds/ stream segments. Along the traverse, the major knickpoints are KP1 ($\sim 1770\text{m}$), KP2 ($\sim 1700\text{m}$), KP3 ($\sim 1150\text{m}$) and KP5 ($\sim 800\text{m}$) respectively (Fig.6). Two minor knickpoints are there- KP4 ($\sim 1000\text{m}$) and KP6 ($\sim 650\text{m}$).

Already Nennewitz et al., (2018) had proposed a high basin-averaged k_{sn} value of > 300 in the KW. Here in this study, we worked with a much-detailed DEM and stream-specific k_{sn} allocation (Fig.7d), as well as a basinwide steepness calculation. Our results corroborate with the earlier findings, but, predict the zone of interest in greater detail. It is important to note that by

setting a higher tolerance level in the ‘knickpointfinder’ tool in Topotoolbox, we have managed to remove the DEM artifacts from consideration (Schwanghart and Scherler, 2014).

4.2.2. Channel width and valley morphology

The channel width of the Chenab River is on average low (30-60m) within the core of the KW (Fig. 3b, 7b), and the low channel width continues till the Chenab River flows N-S along the western margin of the KW. However, there are a few exceptions; upstream from the knickpoint KP1 in the Padder valley (in which the town of Padder is located), the channel widens (width ~80-100m) and the channel gradient is low (Fig. 3a). The second instance of a wider channel is seen upstream from knickpoint KP3, where there is a reservoir for the Dul-Hasti dam. Downstream from KP3 within the Higher Himalaya, the channel width ranges from 50-70 m. However, towards the lower stretches of the N-S traverse, the width is even lower (16-52m). The river width increases to 100-200m as Chenab River takes a westward path thereafter. The channel width increases beyond 300m until it leaves the crystalline rocks in the hanging wall of the MCT and enters the Lesser Himalaya in the hanging wall of the MBT across the Baglihar dam. Within the frontal LH, the channel width is again lowered (50-80 m).

4.2.3. Changes in specific stream power (SSP)

Discharge-normalized SSP data calculated from the upstream stretches and the knickzones, KZ1 and KZ2 show major increase in SSP within the steep knickzones. The increase in SSP from upstream to the knickzones KZ1 and KZ2 are 4.44 and 5.02 times, respectively (Table 1). Such high increase in SSP is aided by steepening of channel gradient (Fig.7c) and narrowing of channel bed (Fig.7b).

4.3. Luminescence chronology

The results for the luminescence chronology ~~experiment~~ are listed in Table 2. Samples collected from the fluvioglacial sediments overlain by debris flow deposit, namely as, K07, K08 and K09, yield IRSL ages of 104.5 ± 5.9 kyr, 114.4 ± 6.3 kyr, and 119.2 ± 6.8 kyr, respectively. Fading corrections done for samples K07 and K09 yield the correction factors (g%) of 0.89 and 1.11 respectively. The sample K08 has not been treated for fading correction, but for easier understanding, we have assumed a constant sedimentation rate between the samples K07 and K09 and extrapolated the 'fading-corrected' age for K08. The oldest sample K09 (132 ± 7 kyr) (fading-corrected IRSL age) is succeeded by samples K08 (126 ± 6 kyr) and K07 (113 ± 6 kyr) respectively. The finer fraction of the hillslope debris overlying the fluvio-glacial deposits yield OSL ages of 81.1 ± 4.6 kyr (K02) and 85 ± 5 kyr (K11) (Fig.6). OSL samples taken from sparsely-preserved sediment layers above the T3 strath surface shows heterogeneous bleaching and hence we provide a minimum age of 22.8 ± 2.1 kyr (sample K16) and 20.5 ± 1.0 kyr (sample K17). One sample taken above T1 strath level is saturated and shows a minimum age of 52.1 ± 2.8 kyr (sample K18) (Table 2). OSL samples K01 and K06 taken from sand layers sitting atop the Higher Himalayan bedrock straths near the town of Doda portray depositional ages of 49.8 ± 2.9 kyr and 51.6 ± 2.4 kyr, respectively (Table 2).

5. Discussions

Analysis of morphometric parameters are widely used as indicators of active tectonics and transient topography (Kirby and Whipple, 2012; Seeber and Gornitz, 1983). Many studies have used morphometry as a proxy for understanding the spatial distribution of active deformation across certain segments of the Himalayan front (Malik and Mohanty, 2007; van der

Beek et al., 2016; Nennewitz et al., 2018; Kaushal et al., 2017). More importantly, some studies have integrated morphometric analysis with chronological constraints to assess the spatial and temporal variability in deformation within the Sub-Himalaya (Lave and Avouac, 2000; Thakur et al., 2014; Vassalo et al., 2015; Dey et al., 2016; Srivastava et al., 2018). All these studies have demonstrated the applicability of morphometric indicators as an estimate of changes in uplift rate or spatial variations of deformation across different landscapes.

Previously-published young Apatite fission-track cooling ages (~ 2-3 Myr) have been interpreted as the result of rapid exhumation of the LH duplex over 10^6 -year timescale (Gavillot et al., 2018). However, how and where the deformation is accommodated across the KW over the 10^3 - 10^5 -year timescale is unknown. In this section, we discuss the obtained morphometric and fluvial characteristics of the studied region and compare these to existing models of deformation. We also discuss how our new luminescence chronological estimates from the transiently-stored sediment archive help us to constrain fluvial incision rates over Late Pleistocene- Holocene timescale and put them in context to regional tectonic deformation models- 1. Mid-crustal ramp model vs. 2. Out-of-sequence fault model.

5.1. Knickpoints and their genesis

Already Seeber and Gornitz (1983) had recognized along the Chenab River is characterized by a zone of steep channel gradient in the vicinity of the KW. Nennewitz et al., (2017) demonstrated a strong correlation between steeped longitudinal river profiles and young thermochronological cooling ages, suggesting recent focused rock uplift and rapid exhumation along many major rivers draining the southern Himalayan front. Although, it is still an open debate whether uplift and growth of the LH Duplex are triggered solely by slip over the crustal

ramp of the MHT or additional out-of-sequence surface-breaking faults ~~are~~ augmenting it (Herman et al., 2010; Elliot et al., 2016; Whipple et al., 2016).

The longitudinal profile of the lower Chenab traverse (below ~2000 m above MSL) is punctuated by two prominent stretches of knickpoint zones and several minor knickpoints related to change of fluvial gradient (Fig.6). Below we will discuss the potential cause of formation of those major knickpoints in the context of detailed field observation, ~~of~~ existing field-collected structural and lithological data, geomorphic features, rock strength and channel width information (Fig.7).

5.1.1. Lithologically-controlled knickpoints

Our findings show that the ~~The~~ Himalayan traverse of the Chenab River is characterized by large variations in substrate lithology and rock strength, which cause variations in the fluvial erodibility and form knickpoints on the river profile (Fig.1, Fig.7e). An instance of soft-to-hard substrate transition happens across the knickpoint KP1, lying downstream from the Padder valley, at the eastern edge of the KW (Fig.2a). Across KP1, the river enters the over-deepened LH bedrock gorge (R value > 50) after exiting the Padder valley filled with transiently-stored, unconsolidated fluvio-glacial sediments (Fig. 3a). A similar soft-to-hard substrate transition is observed upstream from the MCT shear zone. The corresponding knickpoint KP5 represents a change in lithological formation from the sheared and deformed Higher Himalayan crystalline (R value ~35-40) to deep-seated Haimantas (R value ~40-50). There is no field evidence, such as fault splays or ramps, in support of KP5 ~~to be a structurally-controlled one~~.

5.1.2. Tectonically-controlled knickpoints

Compiling previously-published data on regional tectonogeomorphic attributes (Gavillot et al., 2018) with detailed field documentation of structural styles and tectonic features, we

identified several stretches where variations in morphometric proxies indicate spatial variability in rock uplift and faulting across the KW. We have found at least two instances where knickzones are not related to change in substrate, nor are they artificially altered such as constructed dam sites.

The knickzone KZ1 (upstream marked by KP2 ~1700 m above MSL) represents the upstream reach of a steepened river-segment that represents a drop of ~420m of the Chenab River across a run-length of ~15-20 km (Fig.8c). The upstream and downstream side of KP2 is characterized by a change in dip of the LH bedrock foliation (Fig. 2f, 2g, 8) and channel width (Fig. 7b). KP2 also reflects a change in the channel width (Fig. 7b). Interestingly, the steep segment exhibits a narrower channel and particularly steep valley-walls through the core of the KW. Near the end of the steep segment, intensely-deformed (folded and fractured) LH rocks are exposed (Fig.2d, 2e). We infer two main possibilities for these field observations combined with systematic changes of geomorphic characteristics – (1) it may be related to an active surface-breaking out-of-sequence fault or (2) it may be an inactive fault that defines the floor-thrust of one of the numerous proposed duplex nappes. ~~On the contrary,~~ the observed changes in the geomorphic indices along with stretch of the knickzone KZ1 and observed increase in the bedrock dip angle may well be explained by a ramp on the basal decollement. This explanation is supported by the existence of mid-crustal ramps in the balanced cross-section from Gavillot et al., (2018). However, the structural orientation of the rocks (Fig.8a) differ considerably ~~than the~~ proposed LH duplex in Gavillot et al., (2008) raising questions about the duplex-model. Our field observations are supported by previous studies by ~~Fuchs~~ (1975), Frank et al., (1995) and Stephenson et al., (2000) who argued against duplexing of multiple thrust nappes and favoured internal folding of Chail nappe to explain the tectonic growth and deformation pattern within the

KW. Therefore, we cannot clearly comment whether K1 represents a transition from flat to ramp of the MHT or is it indeed an active out-of-sequence thrust-ramp.

On the other hand, the other knickpoint KP3 at the upstream-head of KZ2 nearly coincides with the exposure of the KT (Fig.6). KP3 cannot be a lithologically-controlled knickpoint as it reflects a hard-to-soft substrate transition from LH rocks (R value > 50) to HH rocks (R value < 45) (Fig. 7e). We acknowledge that just across the point KP3, there are some strong leucosomatic layers within the migmatites (R: 58 ± 3), but in general, the migmatites are also brittle-deformed. The rock strength measurement was not done in the multiply-fractured units as it would show inaccurate values. In the longitudinal profile, KP3 does not represent a sharp slope break because the downstream segment runs parallel to main structures and KW-boundary for ~25-30 km, including the KT. Therefore, we performed an orthogonal projection of the E-W trending traverses of the Chenab River and estimated an orogen-perpendicular drop of the Chenab across KZ2 (Fig. 8c). The truncated profile across KZ2 shows a drop of ~230m of the channel across an orogen-perpendicular run-length of ~5 km. The orogen-parallel stretch of the river exhibits narrow channel width (<30-35m) through moderately hard HH bedrock (R-value: 35-45). The tributaries within this stretch form a significant knickpoint at the confluence with the trunk stream (Fig.3f). These field observations suggest recent rapid uplift of the western margin of the KW. The observed differential uplift of the KW margin is possibly either related to growth of the LH-duplex in the core of the window or by surface expression of another crustal ramp emerging from the MHT (Fig.8d). Both the knickzones, KZ1 and KZ2 are the most-prominent disturbance in the longitudinal profile of the Chenab River and are interpreted to portray spatial distribution of differential uplift due to tectonic deformation..

5.2. Temporal and spatial variation of fluvial incision across the KW

Bedrock incision in the Himalaya is not a continuous process and is rather controlled by temporal variations in sediment flux that usually dictates the thickness of the veneer above the bedrock surfaces over which the rivers flow. Late Pleistocene-Holocene sediment transport studies suggested an overall climatic control on sediment aggradation in the interiors of the Himalayan orogen (e.g., Bookhagen et al., 2005; Scherler et al., 2015; Dey et al., 2016); where, stronger climatic conditions may increase the sediment supply and prompt filling of a river valley. Transiently-stored valley-fills are re-incised once the climate weakens. Often the re-incision phases dissect the bedrock units and form strath surfaces. In Chenab valley, we have documented several stages of valley-fills and fluvial strath surfaces.

5.2.1. Sediment aggradation in Chenab valley

The Chenab valley records a net sediment aggradation and transient filling of entire drainage network in the vicinity of the KW since the onset of the last glacial-interglacial cycle (~130 kyr) till ~80 kyr. Fluvioglacial outwash sediments range from at least ~110-130 kyr, whereas the hillslope debris ranges from ~90 to ~80 kyr (Table 2). The chronology of the sediments is in agreement with the overall stratigraphic order of the sediments across the KW. We observe net fluvial re-incision and formation of bedrock strath surfaces since ~80 kyr and formation of epigenetic gorges (Fig.10).

5.2.2. Drainage re-organization and strath terrace formation along Chenab River

Hillslope debris flow from the high-relief frontal horses of the Lesser Himalayan Duplex overlies the fluvio-glacial sediments stored beneath the Kishtwar surface. We argue that the hillslope debris are paleo-landslide deposits which intervened and dammed the paleo-drainage of the Chenab River, which might have been flowing through an easterly path than now (Fig.9). The Maru River, coming from the northwestern corner of our study area was also joining the

Chenab River at a different location (Fig.9). Our argument is supported by field observation of thick silt-clay layer in the proposed paleo-valley of the Maru River (Fig.9a, 9c). OSL sample (K18) from the silt-clay layer is saturated and hence only provide the minimum age of 52 ± 3 kyr. We suggest that the hillslope sediment flux dammed the flow of the Chenab River and also propagated through the aforesaid wind-gap of the Maru River. The decline in the depositional energy has resulted into reduction of grain-size. Post-hillslope debris flow, the Chenab River also diverted to a new path. The new path of the Chenab River upstream from the confluence with the Maru River is defined by a very narrow channel flowing through the Higher Himalayan bedrock gorge (Fig.7b). Downstream from the confluence, we are able to identify at least three levels of strath terraces lying at heights of ~280-290m (T1), ~170m (T2) and ~120m (T3), respectively (Fig.3g,10a). Our field observation suggests that the formation of the straths is at least ~52 kyr-old. The luminescence chronology samples in this study belong to the ~150-170m-thick soft sediments that are stored stratigraphically-up from the T1 strath level. Our field observations and chronological estimates suggest that the renewed path of the Chenab River, must have been formed post the hillslope debris flow ~80-90 kyr but before 52 kyr.

5.2.3. Knickpoint marking epigenetic gorge

Epigenetic gorges are common geomorphic features in the high-mountain landscape (Ouimet et al., 2008). Epigenetic gorges form when channels of a drainage system are transiently buried by sediment aggradation and during subsequent re-incision, a new river channel, often into the neighboring bedrock is incised. The N-S traverse of the Chenab River is largely affected by hillslope sediment flux (paleo-landslides and debris flow) from the steep eastern flank. The knickpoint KP4 situated near the village of Janwas, mark one such instance of epigenetic gorge

where the paleo-valley has been filled initially by fluvio-glacial sediments and the channel abandonment was caused by landslides and hillslope debris flow prior to 80 kyr (Fig. 4b, 4c).

5. 3. Rapid bedrock incision along Chenab River on Late Pleistocene timescale

Considering the rate of excavation of softer sediments to be at least an order of magnitude higher than the rate of bedrock incision (Kothyari and Juyal, 2013; Sharma et al., 2016), we calculated the minimum bedrock incision rate at the western margin of the KW, using the height of the T1 strath ($\sim 280 \pm 5$ m) and the average age of the sediments from the Hillslope debris flow deposit. It yields a minimum bedrock incision rate of ~ 3.1 - 3.5 mm/yr over the last 80-90 kyr. Considering the saturated OSL sample from the paleo-valley, we estimated the maximum bedrock incision since 52 kyr to be 5.1 - 5.5 mm/yr. Similarly, using the minimum age estimate of the T3 terrace abandonment, we deduce a maximum bedrock incision rate of ~ 5.7 - 6.1 mm/yr since ~ 21 kyr. However, further downstream, away from the KW, the average bedrock incision rate derived from dated strath surfaces ($\sim 36 \pm 2$ m high from the Chenab River) near the town of Doda is 0.7 ± 0.1 mm/yr (sample K01 and K06). We don't have bedrock incision rates from the core and the eastern margin of the KW, as the core is devoid of sediment storage and the eastern margin is filled with fluvio-glacial sediments and the river is incising the fill. These results indicate that despite transient choking of the drainage network by sediments during times of valley aggradation, the topography experienced high incision, when sediment coverage had been completely penetrated and bedrock straths had been created post-renewal of the fluvial flow.

5.4. Our new results in context with the previously-published data

AFT-cooling ages by Kumar et al., (1995) showcased young cooling ages from the core of the KW and its western margin (AFT ages: ~2-3 Myr) compared to the surroundings (AFT age: 6-12 Myr). The calculated high exhumation rates proposed by Gavillot et al., (2018) are based on using a geothermal gradient of 35-40°C/km in Dodson's equation assuming a 1-D model (Dodson, 1973). Additional data and thermal modeling are needed across the KW to constrain the exhumation rates from vertical transect. However, lateral similarities of the regional topography and age patterns along the Sutlej area, Beas and Dhauladhar Range (Thiede et al., 2017; Thiede et al., 2009; Stübner et al., 2018) have yielded similar exhumation rates in the range of 2-3 mm/yr ~~and are confirming obtained rates.~~ Long-term exhumation rates from the NW Himalaya agree well with findings of Nennevit et al. (2018) who correlated the young thermochron ages with high basinwide k_{sn} values suggesting high uplift rates over intermediate to longer timescales. Although the geomorphic implications on landscape evolution provide resolution at shorter timescales than the low-T thermochron studies, our field observations and analysis support very well a protracted long-term uplift rates across the KW. Interestingly, exhumation rates steepened stretches is nearly one order of magnitude higher than that of the Higher Himalayan units in the klippe. Our estimates of SSP also reflect an increase by ~five times within the steepened stretches.

5.5. Two competing models: duplex-growth model vs. out-of-sequence fault-ramp model

Deeply-incised channel morphology, steep channel gradients marked by knickpoints at the upstream reaches in and around the KW could be explained by the presence of at least two orogen-parallel mid-crustal ramps on the MHT (Fig.8d). Existence of two mid-crustal ramps has already been shown through sequential balanced cross-sections for the last 10 Myr across the Kashmir Himalaya (Gavillot et al., 2018). The study by Gavillot et al., (2018) focused on duplex

growth model as the balanced cross-section portrays several LH nappes stacked together (Fig. 8d). Translation on the MHT can impart differential uplift of the LH duplex across the two mid-crustal ramps as ramps would show higher uplift/ exhumation due to higher angle of dip of floor-thrust of the duplex. Here we provide more detailed information on spatial distribution of active differential uplift across the KW (Fig.8a, 8d). Our field observation questions the existence of multiple nappes forming a duplex (Gavillot et al., 2018) and rather favors anticlinal doming of the pervasively-deformed Chail nappe, as suggested by Fuchs (1975) and Stephenson et al., (2000). We observe pronounced deformation at the core of the KW (Fig. 2d, 2e) suggesting that this could be related to active faulting, crustal buckling or internal folding which maintain continuous rock-uplift forcing the Chenab River to incise and maintain the steepened stretch of KZ1. Gavillot et al., (2018) proposed that translation on a mid-crustal ramp of the MHT and no surface-faulting is driving the uplift at the core of the KW (Fig.8d). We provide an alternative explanation for the observed steep stream segment at the core of the KW. We speculate the existence of a crustal fault-ramp emerging from the MHT that triggers rapid exhumation of the hanging wall. In that case, out-of-sequence faulting causes high relief, steep channel gradients and higher basinwide steepness indices over the ramp (Fig.7). Similar ramps have been proposed on the MBT beneath the Dhauladhar Range (Thiede et al., 2017) and in the east of the NW Himalaya (Caldwell et al., 2013; Mahesh et al., 2015; Stübner et al., 2018; Yadav et al., 2019). Similar mid-crustal ramp (MCR-2) has been proposed for the western margin of the KW by Gavillot et al., (2018). We don't have any direct field evidence of regional surface-breaking faults which could be related to KZ2. However, rapid fluvial incision, increase in SSP and channel steepness probably justify the existence of either a mid-crustal ramp or an out-of-sequence surface-breaking fault.

Detailed structural mapping and morphometric analysis using high-resolution DEM provide important constraints on the spatial extent of deformation. We are able to resolve the high-relief Kishtwar Window and the surroundings into two major steep orogen-parallel belts/zones (Fig. 5e, 8d) - one at the core of the KW could be an active high-angle fault-ramp emerging from the MHT or a crustal ramp, and the other ~~one~~ observed along the western margin of the KW could be another ramp on the MHT or a surface-breaking back-thrust evolving in relationship to the growth of the LH duplex. More importantly, we demonstrate that the Kishtwar Window is still growing and therefore could be the potential source of future seismic activity.

6. Conclusions

Our field observation and the characteristics of terrain morphology match well with the spatial pattern of previously-published thermochronological data and indicate that the Kishtwar Window is undergoing tectonic deformation, uplift and exhumation at present, on Late Pleistocene-Holocene timescales, and in geological past since at least the late Miocene. By compiling our new results and published records, we favor the following conclusions:

1. The Chenab River maintains an over-steepened bedrock channel and a low channel width irrespective of lithological variations across the KW and beyond, suggesting ongoing rapid fluvial incision related to active tectonic rock uplift.
2. Our field observations, morphometric analysis, and rock strength measurements document that at least two of these major knickzones with steep longitudinal gradients on the trunk stream are non-lithologic and are likely related to

differential rock uplift. The incision potential (specific stream power) in the steepened stretches ~4-5 times higher than the surroundings.

3. The differential uplift can be explained either by slip on the multiple ramps on the MHT and exhumation of the duplex floor-thrust or by a combination of slip on the MHT ramp and active out-of-sequence faulting. As of now, we do not have any evidence for large-scale out-of-sequence faulting.

4. Luminescence chronology of the transiently-stored sediments along the Chenab River suggests that the valley had been overfilled by sediments of fluvio-glacial origin as well as by hillslope sediment flux. Massive sediment aggradation during ~130-80 kyr led to drainage re-organization and bedrock incision leaving behind strath surfaces.

5. The late Quaternary bedrock incision rates near the western margin of the KW are high 3.1-3.6 mm/yr while away from KW, the incision rates are low (< 1 mm/yr).

To summarize, our new study reinforces the importance of detailed field observation, and morphometric analysis in understanding the neotectonic framework of the interiors of the Himalaya. With additional chronological evidence from the transiently-stored sediments, we showcase high rates of bedrock incision in the interior of the western Himalaya, which could potentially be indicative of tectonic control on landscape evolution. However, to solve the debate of ongoing duplex-growth vs. active out-of-sequence faulting, we would require more field data on active structures and chronological constraints on deformation rates across potentially-active structures.

Appendix

Additional maps, figures on morphometric analysis and luminescence dating are listed in

Appendix A. Data of rock strength measurements provided in Table C1. Luminescence sample processing is elaborated in Appendix B.

Code availability

Authors used open-source codes of Topotoolbox and Topographic Analysis Kit Toolbox for this study.

Data availability

Field data are already provided in Appendix 1. Additional data on luminescence dating can be provided on request.

Sample availability

Samples used for luminescence dating are already mostly-destroyed, therefore it is beyond sharing.

Author contribution

S.Dey, the first author, this work and completed the fieldwork, sample processing, measurements and writing of this manuscript. R. Thiede helped in fieldwork, discussion and writing of this manuscript. A. Biswas performed the initial morphometric analysis. N.Chauhan helped in measurement of luminescence signal and assessment of the data. P.Chakravarti performed the channel width calculations and compiled the rock strength measurements. V. Jain helped in discussion and writing of the manuscript.

Competing interests

The authors declare that they have no conflict of interest.

Acknowledgments

This study is funded by the DST INSPIRE faculty fellowship program by the Department of Science and Technology, India (grant #DST/INSPIRE/04/2017/003278), and IIT Gandhinagar post-doctoral research fund (IP/IITGN/ES/SD/201718-01). Thiede is supported by German Science Foundation (grant # DFG TH 1317-8 and 9). We thank M.K.Jaiswal and M.Rawat for providing the elemental analysis. We thank Shambhu Das, Avi Das, Niklas Schaaf, Akashsingh Rajput and Chamel Singh for their assistance during fieldwork. We also thank Soumyajit Mukherjee, Rahul Kaushal and Shantamoy Guha for scientific inputs and comments on this manuscript. We acknowledge A. Forte, Y. Gavillot, S. Hergarten and one anonymous reviewer for their constructive and insightful reviews. We like to thank the editor R. Gloaguen and ~~associate~~ editor A. Joshua West for their help during review process.

References

- Abrahami, R., van der Beek, P., Huyghe, P., Hardwick, E., & Carcaillet, J. (2016). Decoupling of long-term exhumation and short-term erosion rates in the Sikkim Himalaya. *Earth and Planetary Science Letters*, 433, 76-88.
- Bagnold, R. A. (1966). *An approach to the sediment transport problem from general physics*. US government printing office.
- Bhatia, T. R., & Bhatia, S. K. (1973). Sedimentology of the slate belt of Ramban-Banihal area, Kashmir Himalaya. *Himalayan Geology*, 3, 116-134.
- Bollinger, L., Henry, P., & Avouac, J. P. (2006). Mountain building in the Nepal Himalaya: Thermal and kinematic model. *Earth and Planetary Science Letters*, 244(1-2), 58-71.

767 Bookhagen, B., & Burbank, D. W. (2006). Topography, relief, and TRMM-derived rainfall
768 variations along the Himalaya. *Geophysical Research Letters*, 33(8).

769 Bookhagen, B., Thiede, R. C., & Strecker, M. R. (2005). Late Quaternary intensified monsoon
770 phases control landscape evolution in the northwest Himalaya. *Geology*, 33(2), 149-152.

771 Bookhagen, B., Fleitmann, D., Nishiizumi, K., Strecker, M. R., & Thiede, R. C. (2006).
772 Holocene monsoonal dynamics and fluvial terrace formation in the northwest Himalaya,
773 India. *Geology*, 34(7), 601-604.

774 Burbank, D. W., Leland, J., Fielding, E., Anderson, R. S., Brozovic, N., Reid, M. R., & Duncan,
775 C. (1996). Bedrock incision, rock uplift and threshold hillslopes in the northwestern
776 Himalayas. *Nature*, 379(6565), 505.

777 Burgess, W. P., Yin, A., Dubey, C. S., Shen, Z. K., & Kelty, T. K. (2012). Holocene shortening
778 across the Main Frontal Thrust zone in the eastern Himalaya. *Earth and Planetary Science*
779 *Letters*, 357, 152-167.

780 Caldwell, W. B., Klemperer, S. L., Lawrence, J. F., and Rai, S. S., 2013, Characterizing the Main
781 Himalayan Thrust in the Garhwal Himalaya, India with receiver function CCP stacking: *Earth*
782 *and Planetary Science Letters*, v. 367, p. 15-27.

783 Colleps, C. L., Stockli, D. F., McKenzie, N. R., Webb, A. A. G., & Horton, B. K. (2019).
784 Neogene Kinematic Evolution and Exhumation of the NW India Himalaya: Zircon Geo-and
785 Thermochronometric Insights From the Fold-Thrust Belt and Foreland Basin. *Tectonics*, 38(6),
786 2059-2086.

787 DeCelles, P. G., Robinson, D. M., Quade, J., Ojha, T. P., Garzzone, C. N., Copeland, P., and
788 Upreti, B. N., 2001, Stratigraphy, structure, and tectonic evolution of the Himalayan fold-thrust
789 belt in western Nepal: *Tectonics*, v. 20, no. 4, p. 487-509.

790 Deeken, A., Thiede, R. C., Sobel, E. R., Hourigan, J. K., & Strecker, M. R. (2011).
791 Exhumational variability within the Himalaya of northwest India. *Earth Planetary Science Letters*,
792 305(1-2), 103–114. <https://doi.org/10.1016/j.epsl.2011.02.045>

793 Dey, S., Thiede, R. C., Schildgen, T. F., Wittmann, H., Bookhagen, B., Scherler, D., & Strecker,
794 M. R. (2016). Holocene internal shortening within the northwest Sub-Himalaya: Out-of-
795 sequence faulting of the Jwalamukhi Thrust, India. *Tectonics*, 35(11), 2677-2697.

796 Dey, S., Thiede, R. C., Schildgen, T. F., Wittmann, H., Bookhagen, B., Scherler, D., Jain, V., &
797 Strecker, M. R. (2016). Climate-driven sediment aggradation and incision since the late
798 Pleistocene in the NW Himalaya, India. *Earth and Planetary Science Letters*, 449, 321-331.

799 DiPietro, J. A., & Pogue, K. R. (2004). Tectonostratigraphic subdivisions of the Himalaya: A
800 view from the west. *Tectonics*, 23(5).

801 Duvall, A., Kirby, E., & Burbank, D. (2004). Tectonic and lithologic controls on bedrock
802 channel profiles and processes in coastal California. *Journal of Geophysical Research: Earth*
803 *Surface*, 109(F3).

804 Elliott, J. R., Jolivet, R., González, P. J., Avouac, J. P., Hollingsworth, J., Searle, M. P., &
805 Stevens, V. L. (2016). Himalayan megathrust geometry and relation to topography revealed by
806 the Gorkha earthquake. *Nature Geoscience*, 9(2), 174.

807 Eugster, P., Scherler, D., Thiede, R. C., Codilean, A. T., and Strecker, M. R., (2016). Rapid Last
808 Glacial Maximum deglaciation in the Indian Himalaya coeval with midlatitude glaciers: New
809 insights from ^{10}Be -dating of ice-polished bedrock surfaces in the Chandra Valley, NW
810 Himalaya: *Geophysical Research Letters*, v. 43, no. 4, p. 1589-1597.

811 Finnegan, N. J., Roe, G., Montgomery, D. R., & Hallet, B. (2005). Controls on the channel width
812 of rivers: Implications for modeling fluvial incision of bedrock. *Geology*, 33(3), 229-232.

813 Flint, J. J. (1974). Stream gradient as a function of order, magnitude, and discharge. *Water*
814 *Resources Research*, 10(5), 969-973.

815 Forte, A.M. and Whipple, K.X. (2019). The Topographic Analysis Toolkit (TAK) for
816 Topotoolbox. *Earth Surface Dynamics*, 7, 87-95.

817 Frank, W., Grasemann, B., Guntli, P. E. T. E. R., & Miller, C. (1995). Geological map of the
818 Kishtwar-Chamba-Kulu region (NW Himalayas, India). *Jahrbuch der Geologischen*
819 *Bundesanstalt*, 138(2), 299-308.

820 Fuchs, G. (1975). Contributions to the geology of the North-Western Himalayas. *Geologische*
821 *Bundesanstalt*.

822 Fuchs, G. (1981). Outline of the geology of the Himalaya. *Mitt. osterr. geol. Ges*, 74(75), 101-
823 127.

824 Gavillot, Y. G. (2014). Active tectonics of the Kashmir Himalaya (NW India) and earthquake
825 potential on folds, out-of-sequence thrusts, and duplexes.

826 Gavillot, Y., Meigs, A. J., Sousa, F. J., Stockli, D., Yule, D., & Malik, M. (2018). Late Cenozoic
827 Foreland-to-Hinterland Low-Temperature Exhumation History of the Kashmir
828 Himalaya. *Tectonics*.

829 Gavillot, Y., Meigs, A., Yule, Y., Heermance, R., Rittenour, T., Madugo, C., & Malik, M.
830 (2016). Shortening rate and Holocene surface rupture on the Riasi fault system in the Kashmir
831 Himalaya: Active thrusting within the Northwest Himalayan orogenic wedge. *Geological Society*
832 *of America Bulletin*, 128(7-8), 1070–1094. <https://doi.org/10.1130/B31281.1>

833 Harvey, J. E., Burbank, D. W., & Bookhagen, B. (2015). Along-strike changes in Himalayan
834 thrust geometry: Topographic and tectonic discontinuities in western Nepal. *Lithosphere*, 7(5),
835 511-518.

836 Herman, F., Copeland, P., Avouac, J.P., Bollinger, L., Mahéo, G., Le Fort, P., Rai, S., Foster, D.,
837 Pêcher, A., Stüwe, K. and Henry, P., 2010. Exhumation, crustal deformation, and thermal
838 structure of the Nepal Himalaya derived from the inversion of thermochronological and
839 thermobarometric data and modeling of the topography. *Journal of Geophysical Research: Solid*
840 *Earth*, 115(B6).

841 Hirschmiller, J., Grujic, D., Bookhagen, B., Coutand, I., Huyghe, P., Mugnier, J.-L., and Ojha,
842 T., 2014, What controls the growth of the Himalayan foreland fold-and-thrust belt?: *Geology*, v.
843 42, no. 3, p. 247-250.

844 Kaushal, R. K., Singh, V., Mukul, M., & Jain, V. (2017). Identification of deformation
845 variability and active structures using geomorphic markers in the Nahan salient, NW Himalaya,
846 India. *Quaternary International*, 462, 194-210.

847 Kumar, A., Lal, N., Jain, A. K., & Sorkhabi, R. B. (1995). Late Cenozoic–Quaternary thermo-
848 tectonic history of Higher Himalayan Crystalline (HHC) in Kishtwar–Padar–Zaskar region,
849 NW Himalaya: Evidence from fission-track ages. *Journal of the Geological Society of India*,
850 45(4), 375–391.

851 Kundu, B., Yadav, R. K., Bali, B. S., Chowdhury, S., & Gahalaut, V. K. (2014). Oblique
852 convergence and slip partitioning in the NW Himalaya: implications from GPS
853 measurements. *Tectonics*, 33(10), 2013–2024.

854 Lavé, J., & Avouac, J. P. (2000). Active folding of fluvial terraces across the Siwaliks Hills,
855 Himalayas of central Nepal. *Journal of Geophysical Research: Solid Earth*, 105(B3), 5735–5770.

856 Lavé, J., & Avouac, J. P. (2001). Fluvial incision and tectonic uplift across the Himalayas of
857 central Nepal. *Journal of Geophysical Research: Solid Earth*, 106(B11), 26561–26591.

858 Mahesh, P., Gupta, S., Saikia, U., and Rai, S. S., 2015, Seismotectonics and crustal stress field in
859 the Kumaon-Garhwal Himalaya: *Tectonophysics*, v. 655, p. 124–138.

860 Malik, J. N., & Mohanty, C. (2007). Active tectonic influence on the evolution of drainage and
861 landscape: geomorphic signatures from frontal and hinterland areas along the Northwestern
862 Himalaya, India. *Journal of Asian Earth Sciences*, 29(5–6), 604–618.

863 Miller, J. R. (1991). The influence of bedrock geology on knickpoint development and channel-
864 bed degradation along downcutting streams in south-central Indiana. *The Journal of*
865 *Geology*, 99(4), 591–605.

866 Mitra, G., Bhattacharyya, K., & Mukul, M. (2010). The lesser Himalayan duplex in Sikkim:
867 implications for variations in Himalayan shortening. *Journal of the Geological Society of*
868 *India*, 75(1), 289-301.

869 Montgomery, D. R., & Brandon, M. T. (2002). Topographic controls on erosion rates in
870 tectonically active mountain ranges. *Earth and Planetary Science Letters*, 201(3-4), 481-489.

871 Mukherjee S. (2015) A review on out-of-sequence deformation in the Himalaya. In: Mukherjee
872 S, Carosi R, van der Beek P, Mukherjee BK, Robinson D (Eds) *Tectonics of the*
873 *Himalaya*. Geological Society, London. Special Publications 412, 67-109.

874 Nábělek, J., Hetényi, G., Vergne, J., Sapkota, S., Kafle, B., Jiang, M., Su, H., Chen, J., & Huang,
875 B. S. (2009). Underplating in the Himalaya-Tibet collision zone revealed by the Hi-CLIMB
876 experiment. *Science*, 325(5946), 1371-1374.

877 Nadim, F., Kjekstad, O., Peduzzi, P., Herold, C., & Jaedicke, C. (2006). Global landslide and
878 avalanche hotspots. *Landslides*, 3(2), 159-173.

879 Nennevitz, M., Thiede, R. C., & Bookhagen, B. (2018). Fault activity, tectonic segmentation,
880 and deformation pattern of the western Himalaya on Ma timescales inferred from landscape
881 morphology. *Lithosphere*, 10(5), 632-640.

882 Ni, J., and M. Barazangi (1984), Seismotectonics of the Himalayan collision zone: Geometry of
883 the underthrusting Indian plate beneath the Himalaya, *J. Geophys. Res.*, 89, 1147 – 1163.

884 Powers, P. M., Lillie, R. J., & Yeats, R. S. (1998). Structure and shortening of the Kangra and
885 Dehra Dun reentrants, sub-Himalaya, India. *Geological Society of America Bulletin*, 110(8),
886 1010-1027.

887 Raiverman, V. (1983). Basin geometry, Cenozoic sedimentation and hydrocarbon prospects in
888 north western Himalaya and Indo-Gangetic plains. *Petroleum Asia Journal: Petroliferous basins*
889 of India, 6(4), 67-92.

890 Robert, X., Van Der Beek, P., Braun, J., Perry, C., Dubille, M., & Mugnier, J. L. (2009).
891 Assessing Quaternary reactivation of the Main Central thrust zone (central Nepal Himalaya):
892 New thermochronologic data and numerical modeling. *Geology*, 37(8), 731-734.

893 Robinson, D. M., & Martin, A. J. (2014). Reconstructing the Greater Indian margin: A balanced
894 cross section in central Nepal focusing on the Lesser Himalayan duplex. *Tectonics*, 33(11), 2143-
895 2168.

896 Royden, L., & Taylor Perron, J. (2013). Solutions of the stream power equation and application
897 to the evolution of river longitudinal profiles. *Journal of Geophysical Research: Earth*
898 *Surface*, 118(2), 497-518.

899 Scherler, D., Bookhagen, B., Wulf, H., Preusser, F., & Strecker, M. R. (2015). Increased late
900 Pleistocene erosion rates during fluvial aggradation in the Garhwal Himalaya, northern
901 India. *Earth and Planetary Science Letters*, 428, 255-266.

902 Schwanghart, W., & Scherler, D. (2014). TopoToolbox 2—MATLAB-based software for
903 topographic analysis and modeling in Earth surface sciences. *Earth Surface Dynamics*, 2(1), 1-7.

904 Searle, M. P., Stephenson, B., Walker, J., & Walker, C. (2007). Restoration of the Western
905 Himalaya: implications for metamorphic protoliths, thrust and normal faulting, and channel flow
906 models. *Episodes*, 30(4), 242.

907 Seeber, L., & Gornitz, V. (1983). River profiles along the Himalayan arc as indicators of active
 908 tectonics. *Tectonophysics*, 92(4), 335-367.

909 Snyder, N. P., Whipple, K. X., Tucker, G. E., & Merritts, D. J. (2000). Landscape response to
 910 tectonic forcing: Digital elevation model analysis of stream profiles in the Mendocino triple
 911 junction region, northern California. *Geological Society of America Bulletin*, 112(8), 1250-1263.

912 Steck, A. (2003). Geology of the NW Indian Himalaya. *Eclogae Geol Helv*, 96, 147-196.

913 Stephenson, B. J., Waters, D. J., & Searle, M. P. (2000). Inverted metamorphism and the Main
 914 Central Thrust: field relations and thermobarometric constraints from the Kishtwar Window, NW
 915 Indian Himalaya. *Journal of Metamorphic Geology*, 18(5), 571-590.

916 Stevens, V. L., & Avouac, J. P. (2015). Interseismic coupling on the main Himalayan
 917 thrust. *Geophysical Research Letters*, 42(14), 5828-5837.

918 Stübner, K., Grujic, D., Dunkl, I., Thiede, R., & Eugster, P. (2018). Pliocene episodic
 919 exhumation and the significance of the Munsiri thrust in the northwestern Himalaya. *Earth and*
 920 *Planetary Science Letters*, 481, 273-283.

921 Thakur, V. C. (Ed.). (1992). *Geology of western Himalaya* (Vol. 19). Pergamon Press.

922 Thakur, V. C., Joshi, M., Sahoo, D., Suresh, N., Jayangondapermal, R., & Singh, A. (2014).
 923 Partitioning of convergence in Northwest Sub-Himalaya: estimation of late Quaternary uplift and
 924 convergence rates across the Kangra reentrant, North India. *International Journal of Earth*
 925 *Sciences*, 103(4), 1037-1056.

926 Thiede, R., Robert, X., Stübner, K., Dey, S., & Faruhn, J. (2017). Sustained out-of-sequence
 927 shortening along a tectonically active segment of the Main Boundary thrust: The Dhauladhar
 928 Range in the northwestern Himalaya. *Lithosphere*, 9(5), 715-725.

929 Thiede, R. C., Bookhagen, B., Arrowsmith, J. R., Sobel, E. R., & Strecker, M. R. (2004).
 930 Climatic control on rapid exhumation along the southern Himalayan Front. *Earth and Planetary*
 931 *Science Letters*, 222(3-4), 791–806. <https://doi.org/10.1016/j.epsl.2004.03.015>

932 Turowski, J. M., Lague, D., and Hovius, N. (2009). Response of bedrock channel width to
 933 tectonic forcing: Insights from a numerical model, theoretical considerations, and comparison
 934 with field data. *Journal of Geophysical Research: Earth Surface*, 114(F3).

935 Vassallo, R., Mugnier, J. L., Vignon, V., Malik, M. A., Jayangondaperumal, R., Srivastava, P.,
 936 and Carcaillet, J. (2015). Distribution of the late-Quaternary deformation in northwestern
 937 Himalaya. *Earth and Planetary Science Letters*, 411, 241-252.

938 Wadia, D. N. (1934). The Cambrian-Trias sequence of north-western Kashmir (parts of
 939 Muzaffarabad and Baramula districts). *Records of the Geological Survey of India*, 68(2), 121-
 940 176.

941 Webb, A. A. G., Yin, A., Harrison, T. M., Célérier, J., Gehrels, G. E., Manning, C. E., & Grove,
 942 M. (2011). Cenozoic tectonic history of the Himachal Himalaya (northwestern India) and its
 943 constraints on the formation mechanism of the Himalayan orogen. *Geosphere*, 7(4), 1013-1061.

944 Wesnousky, S. G., Kumar, S., Mohindra, R., & Thakur, V. C. (1999). Uplift and convergence
 945 along the Himalayan Frontal Thrust of India. *Tectonics*, 18(6), 967-976.

946 Whipple, K. X., & Tucker, G. E. (1999). Dynamics of the stream-power river incision model:
 947 Implications for height limits of mountain ranges, landscape response timescales, and research
 948 needs. *Journal of Geophysical Research: Solid Earth*, 104(B8), 17661-17674.

949 Whipple, K. X., DiBiase, R. A., & Crosby, B. T. (2013). Bedrock rivers. In *Treatise on*
 950 *geomorphology*. Elsevier Inc..

951 Wobus, C. W., Hodges, K. V., & Whipple, K. X. (2003). Has focused denudation sustained
 952 active thrusting at the Himalayan topographic front?. *Geology*, 31(10), 861-864.

953 Wobus, C., Heimsath, A., Whipple, K., & Hodges, K. (2005). Active out-of-sequence thrust
 954 faulting in the central Nepalese Himalaya. *Nature*, 434(7036), 1008.

955 Wobus, C., Whipple, K. X., Kirby, E., Snyder, N., Johnson, J., Spyropolou, K., Crosby, B.,
 956 Sheehan, D & Willett, S. D. (2006). Tectonics from topography: Procedures, promise, and
 957 pitfalls. *Special papers-geological society of America*, 398, 55.

958 Yadav, R. K., Gahalaut, V. K., Bansal, A. K., Sati, S., Catherine, J., Gautam, P., Kumar, K., and
 959 Rana, N., 2019, Strong seismic coupling underneath Garhwal–Kumaun region, NW Himalaya,
 960 India: *Earth and Planetary Science Letters*, v. 506, p. 8-14.

961 Yin, A., & Harrison, T. M. (2000). Geologic evolution of the Himalayan-Tibetan orogen. *Annual*
 962 *Review of Earth and Planetary Sciences*, 28(1), 211-280.

963

964 **Figure captions**

965

Figure 1: (a) An overview geological map of the western sector of the Indian Himalaya showing major lithology (modified after Steck, 2003 and Gavillot et al., 2018) and existing structures (Vassalo et al., 2015; Gavillot et al., 2018). The tectonic Kishtwar Window (KW) is surrounded by exposure of MCT, locally known as the Kishtwar Thrust (KT), and exposes the Lesser Himalayan nappes. The Lesser Himalaya forms a west-verging asymmetric anticline. Apatite fission-track (AFT) ages are adapted from Kumar et al., (1995). (b) A balanced cross-section of the NW Himalaya showing the general architecture of the Himalayan orogenic wedge (modified after Gavillot et al., 2018). Note that, beneath the KW, Gavillot et al., (2018) proposed the existence of at least two crustal ramps (MCR-1 and MCR-2) on the MHT, translation on which may have resulted in 3.2-3.6 mm/yr Quaternary exhumation rates across the KW.

Figure 2: Lithological units and structural orientations observed in the Chenab valley. (a) Steeply-dipping HHCS units near the western margin of the KW. (b) Highly-deformed migmatites at the base of the KT. (c) Sub-vertical quartzite slabs of Chail Formation exposed in the frontal horses of the LH Duplex (or, anticline). (d) Highly-deformed, sub-vertical and pervasively folded and compressed quartzite layers within the core of the KW, the base of stacked LH-nappes forming the hanging wall of the proposed surface-breaking fault (Fig. 8d). (e) A close-up view of the folded quartzite units. (f) Steeply-dipping units of granite which formed new penetrative foliation outcropping upstream from the fault-zone. (g) Further upstream from the fault-zone, the bedrocks are gentler in the eastern edge of the KW.

Figure 3: ~~Figure 3:~~ Geomorphic features observed along the Chenab River across the KW. (a) Where the Chenab River enters the KW, the major tributaries coming from the Zansar Range in the north are characterized by ‘U-shaped’ valley suggesting repeated glacial occupancy during the Quaternary. The Chenab valley is unusually wide here providing space for transient storage

989 of glacial outwash sediments. The present-day River re-incises these sedimentary fills.
 990 Photograph was taken near the town of Padder (cf. Fig.1a). (b) At the core of the KW, the
 991 Chenab valley is V-shaped, ~~steep~~ The Chenab River is steep and maintains a narrow channel
 992 width. (c) Highly-elevated fluvial strath surfaces are preserved in the vicinity of the town of
 993 Kishtwar Fluvial incision observed along the N-S traverse of the Chenab River. Photograph was
 994 taken from south of the Kishtwar town. The Kishtwar surface (~400m high from the river) is
 995 underlain by ~150-170m thick sediment cover overlying the tilted Higher Himalayan bedrock.
 996 The River has incised another ~240m bedrock in this section. (d) Epigenetic gorge formed along
 997 the Chenab River in its² N-S traverse through the HHCS. The town of Drabshalla is built on the
 998 hillslope deposits. (e) Chenab River maintained very narrow channel (width: ~20-25 m) through
 999 moderately-strong HHCS rocks, suggesting tectonic imprint on topography. (f) Formation of
 1000 knickpoint at the confluence of the tributary with the trunk stream implying rapid fluvial incision
 1001 of the trunk stream. (g) Three levels of strath surfaces observed below the Kishtwar surface. The
 1002 strath levels are marked as T1 (~280m), T2 (~170m) and T3 (~120m). OSL dating of fluvial
 1003 sediments lying above the T3 surface yield a minimum depositional age of $\sim 21.6 \pm 2.6$ ky.
 1004 **Figure 4:** (a) Lithological distribution near the western margin of the KW (cf. Fig.8 for
 1005 location). Luminescence sample (OSL and IRSL) locations and respective depositional ages (in
 1006 kyr) are shown. Every sample except K16 and K17 ~~are~~ taken above strath level T1. K16 and
 1007 K17 ~~are~~ taken from above the T3 level. Note that, the ages reported in italics are minimum age
 1008 estimates. (b) A field photograph from the village Janwas, south of the town of Kishtwar,
 1009 showing the aggraded sediments lying above the Higher Himalayan tilted bedrock units. (c)
 1010 IRSL ages (in kyr) from the fluvio-glacial sediments and OSL age (in kyr) from the hillslope
 1011 debris units suggest the valley aggradation probably started at the transition of the glacial to

interglacial phase ~120-130 kyr and continued till ~80 kyr ago. (d) A close-up view (red rectangle in fig.4c) of the tilted fluvioglacial sediment layers showing alternate conglomerate and medium-coarse sand layers. (e) A ~3m thick fine sand layer within the hillslope debris yield depositional age of $\sim 86 \pm 5$ kyr. Photograph was taken near the village Pochal, northwest of the town of Kishtwar.

Figure 5: Regional variations in (a) topography, (b) topographic relief (moving window of ~4 km) (c) TRMM-derived rainfall (after Bookhagen and Burbank, 2006), and (d) Basinwide Normalized steepness indices (ksn value) of the region shown dashed box in Figure 1a. (e) Swath profiles (swath window: 50 km) along the line AB (cf. Fig.5a) demonstrate the orogen-perpendicular variations in elevation, rainfall and ksn value. KW is characterized by high elevation, high relief and high steepness, but low rainfall.

Figure 6: Longitudinal profile of the Chenab River show major changes in channel gradient associated with knickpoints in the upstream. It illustrates the major changes in the channel gradient extend over the full length of the KW and strongest changes are located in the core and not at the margins of the window. We classified knickpoints on the basis of their genesis. The substrate lithology along the River is shown. Knickpoints caused by glacial occupancy (G1, G2 and G3) are adapted from Eugster et al.; (2016), who reconstructed the timing of maximum glaciation and extent of glacial cover in source region of upper Chenab River basin during the last glacial maximum. These knickpoints highlight the importance of glacial erosion in the high-elevation sectors, especially in the northern tributaries of the Chenab River. Further in this study, we focused on the area marked by red rectangle.

Figure 7: Along-river variations in (a) channel-elevation, (b) channel width, (c) channel gradient, (d) Normalized steepness index, and (e) rock-strength of non-fractured bedrock units

(R-value taken by rebound hammer) till 165 km upstream from the MBT (point X, cf. Fig.1a). The mean $R\text{-value} \pm \sigma$ for each rock type has been plotted against their spatial extent. We identified two distinct zones (K1 and K2) of high channel gradient and steepness index, which maintain low channel width despite the variable rock strength of the substrate. Knickpoint KP4 may have been generated by the formation of the epigenetic gorge along the N-S traverse of the Chenab River (cf. Fig.3c). Knickpoints KP1 and KP5 mark the transition of a soft-to-hard bedrock substrate.

Figure 8: (a) Detailed structural data from the study area showing structural and lithological variations (modified after Steck, 2003; Gavillot et al., 2018). (b) and (c) orogen-perpendicular drop of the Chenab trunk stream across stretch 1 and stretch 2, respectively, showing transient increase in steepness over the K1 and K2 knickzone. The orthogonal profile projection method has been used in the case of K2 (cf. fig.7) to identify the width of the steep segment. (d) Comparison between two deformation models explaining the observed morphometric variations across the KW – (a) duplex-growth model (adapted from Gavillot et al., 2018) and (b) active out-of-sequence fault model.

Figure 9: A satellite image of the northern Kishtwar town showing the present-day flow-path of the Chenab River (cf. Fig.8 for location). Hillslope debris originated from the steep western margin of the KW (only made of massive white quartzites) and was deposited over fluvio-glacial and glacio-lacustrine sediments and Higher Himalaya schists bedrock exposed below in the Kishtwar valley. Massive hillslope sediment flux impeded the paleo-drainage system leaving behind the paleo-valley of the tributary, the Maru River. Our interpretation of the paleo-drainage is marked in a white dashed line. (a) A view of the Kishtwar surface from the western margin of the KW showing present-day gorge of the Chenab River and its tributary. The wind-gap

(paleo-valley) of the tributary is visible. (b) Thick clay-silt deposit in the wind-gap suggests abandonment of river-flow. The OSL sample is saturated and hence only denotes the minimum age of valley abandonment/ hillslope debris flow. (c) Overview picture of the frontal horses of the LH duplex and the direction of debris flow towards the Kishtwar town. (d) Angular, poorly-sorted clasts and boulders were observed at the base of the debris flow unit near the village of Pochal, north of the Kishtwar town. The white quartzites of LH are exposed in the vicinity of the Kishtwar Town (see satellite image) – only the eastern valley flank can have collapsed in the past.

Figure 10: (a) A topographic and geomorphic profile across the Chenab valley drawn over the Kishtwar Town. The valley aggradation by fluvio-glacial and hillslope debris sediments was succeeded by a fluvial incision which penetrated through the unconsolidated sediments of thickness ~140-150m and incised Higher Himalayan bedrock by $\sim 280 \pm 5$ m, leaving behind at least three recognizable strath surfaces with a thin late Pleistocene sediment cover. The three strath surfaces are at 280 ± 5 m (T1), ~ 170 m (T2), and $\sim 120 \pm 5$ m (T3) heights from the present-day River. We assume that the present-day bedrock gorge has been carved since the deposition of the glacio-lacustrine sediment deposits (~ 100 -130 ky) and the hillslope debris (~ 90 -80 ky) onto former fluvial strath surface of Higher Himalayan Bedrock. The width of the fluvial strath surface where the Kishtwar Town is located indicates that the river network had been dammed earlier too. (b) Graphical representation of mean bedrock incision rates since 80 kyr. Age constraints for T3 are shown in Fig. 4a. Based on relative heights and depositional ages of late Pleistocene deposits, we propose a minimum and a maximum bedrock incision rate of 3.1-3.5 mm/y and 5.2-5.6 mm/yr, respectively. However, further downstream, the bedrock incision rates calculated from bedrock straths farther downstream from the KW range 0.7-0.8 mm/yr.

1081 **Table caption:**

1082 **Table 1:** Calculations of change in specific stream power (SSP) values across the ramp and the
1083 flat segments beneath the LH Duplex. We used a uniform discharge for SSP calculation.

1084 **Table 2:** Sample locations, elemental concentrations, dose rates, equivalent doses and age
1085 estimations for sand samples from Kishtwar valley.

1086

1088

1089



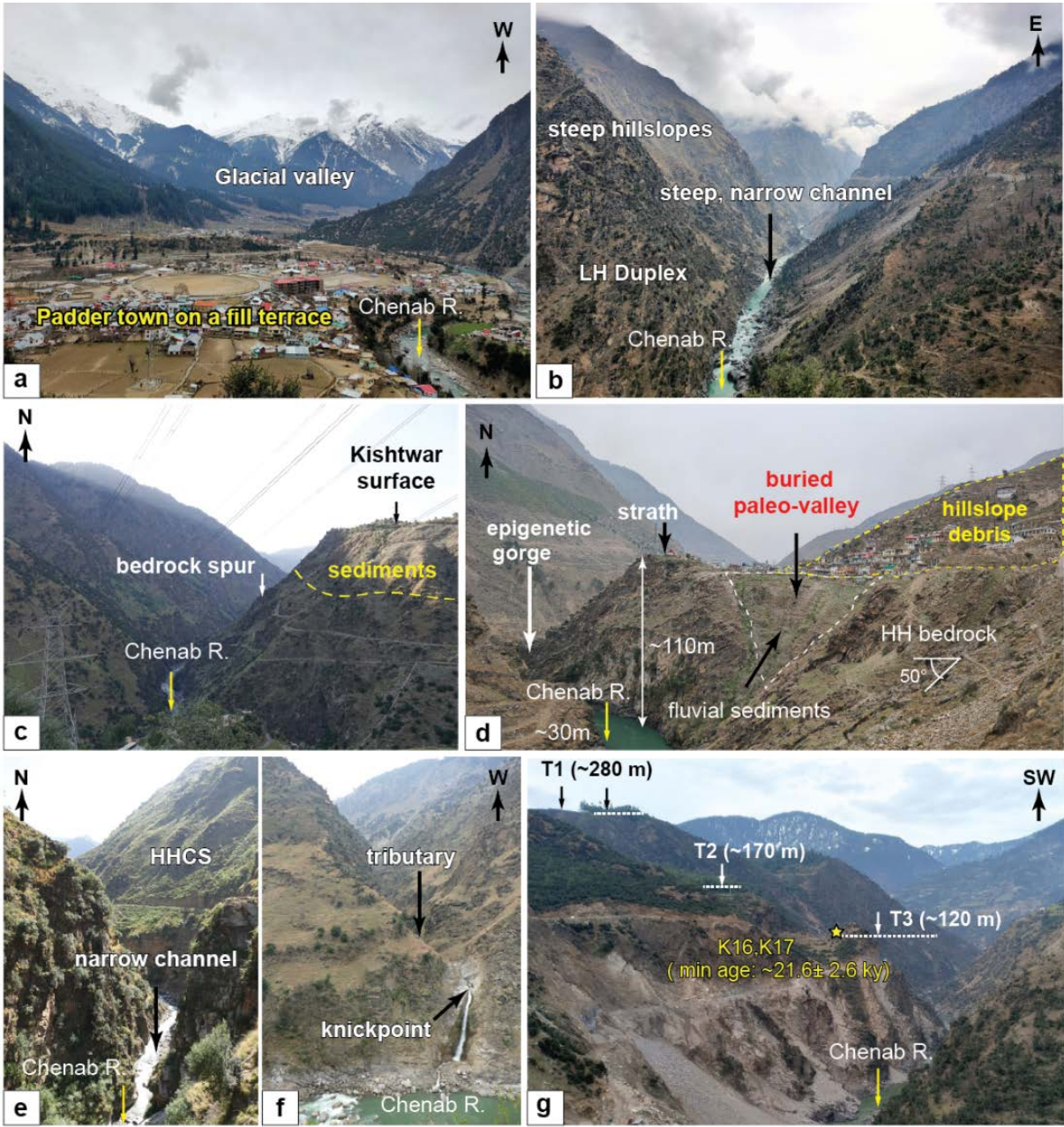
1091

Figure 2



1095

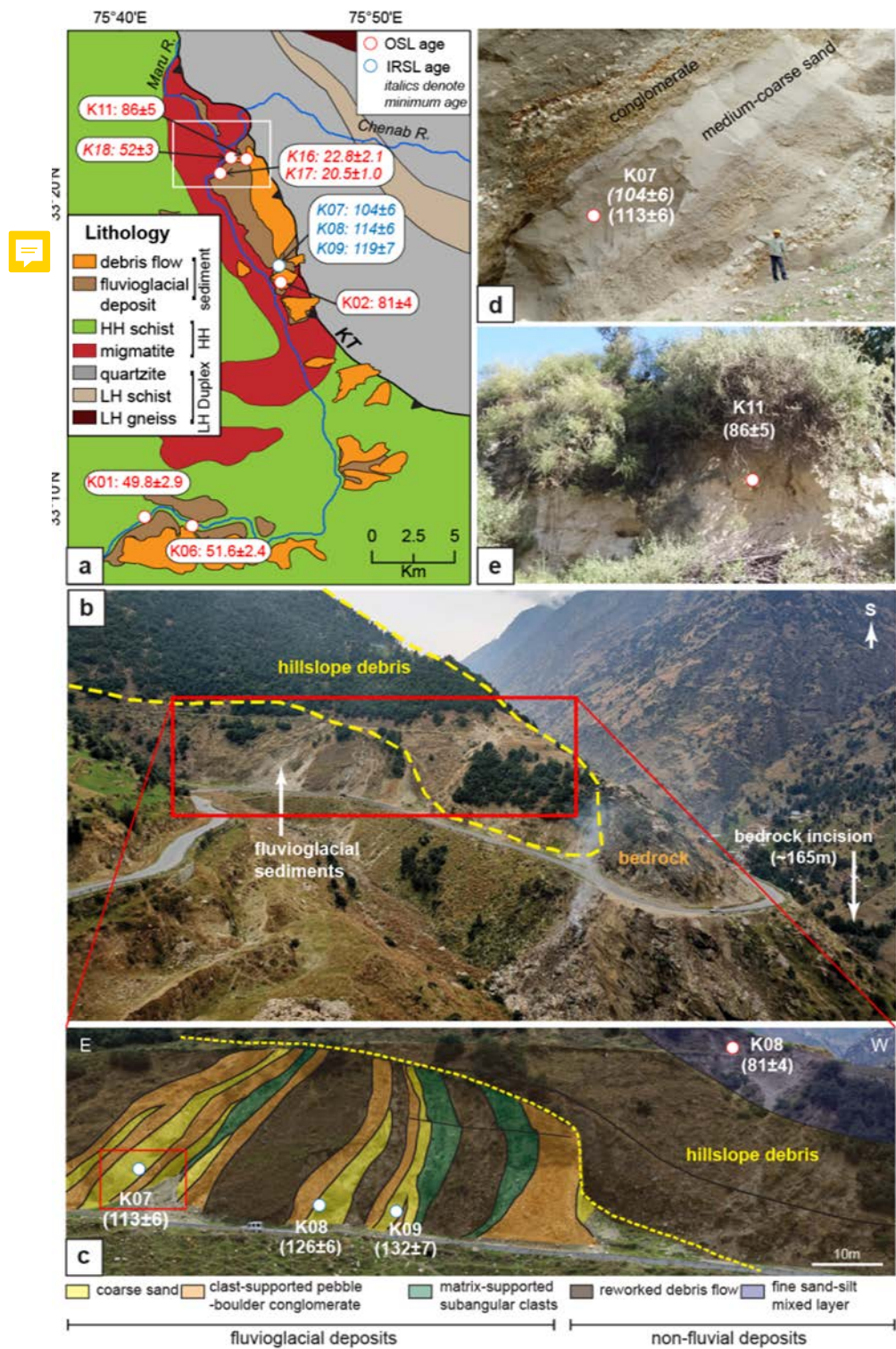
Figure 3



1096

1097

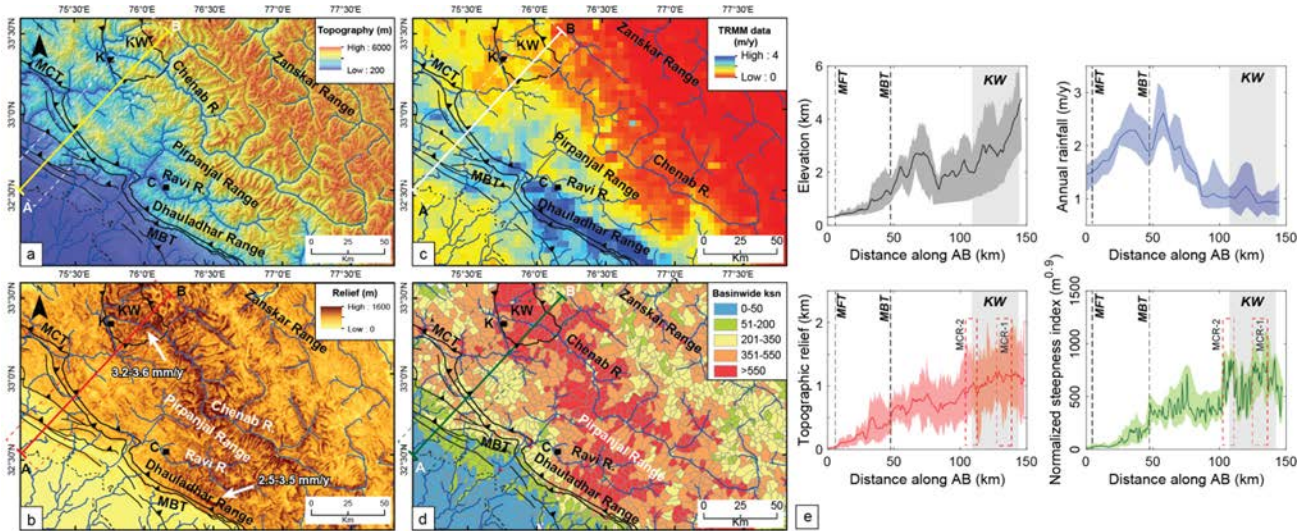
Figure 4



1101



Figure 5

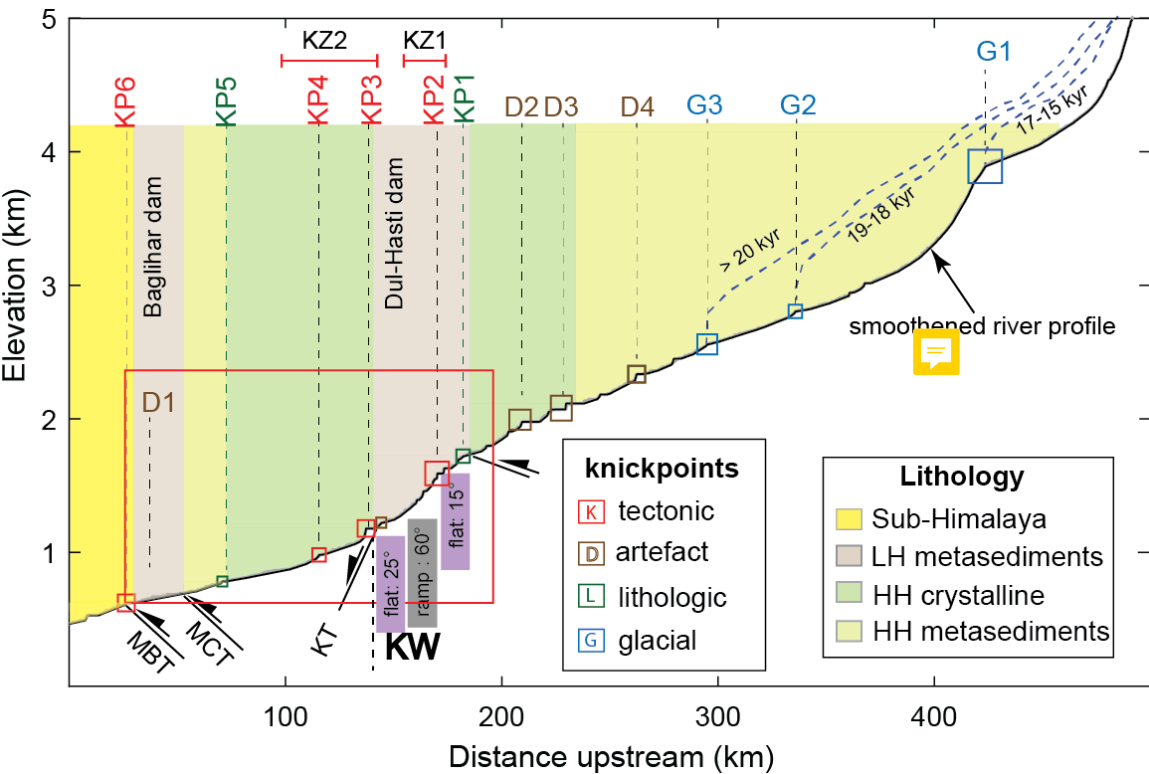


1102

1103

1104

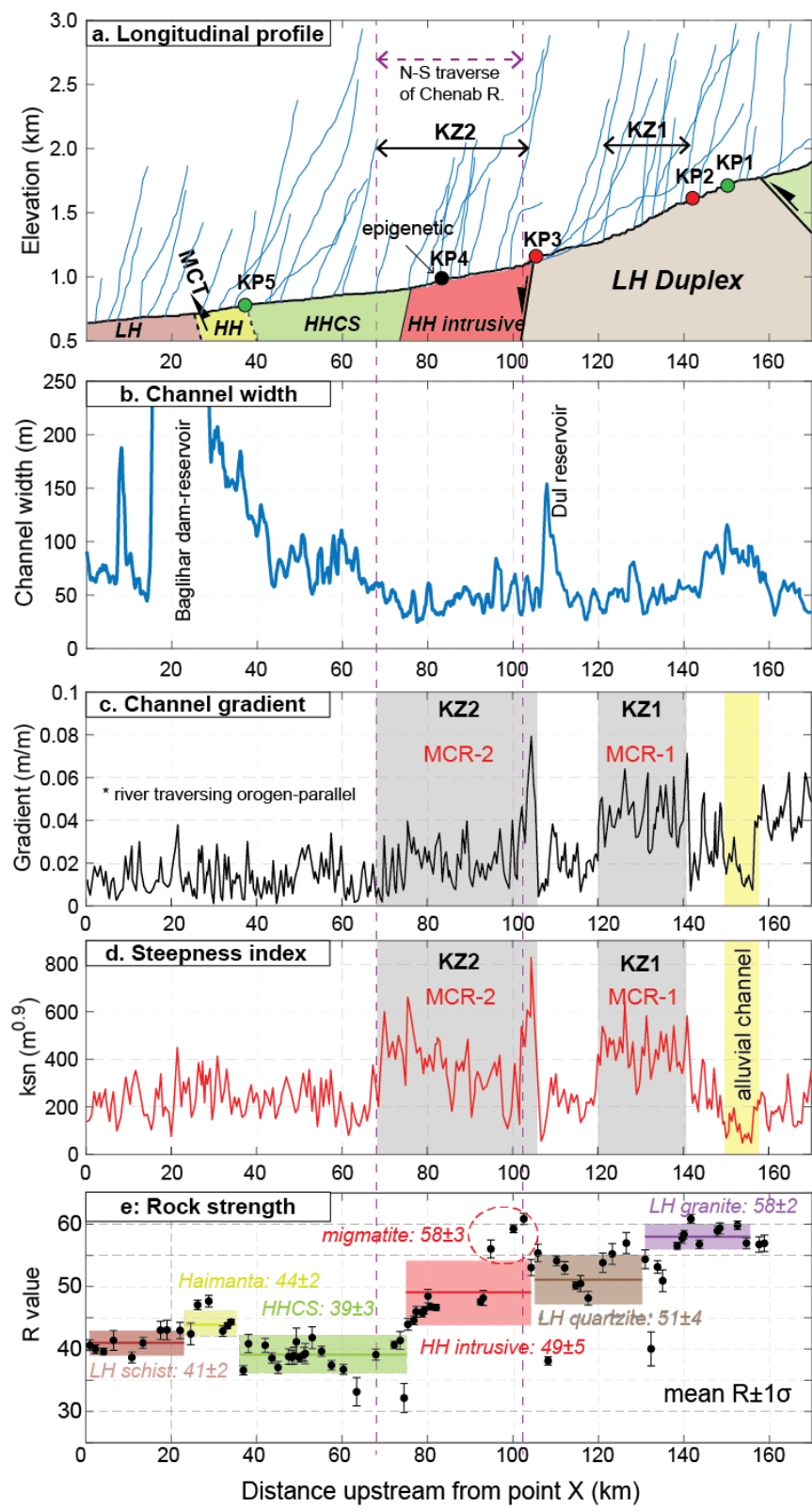
Figure 6



1105

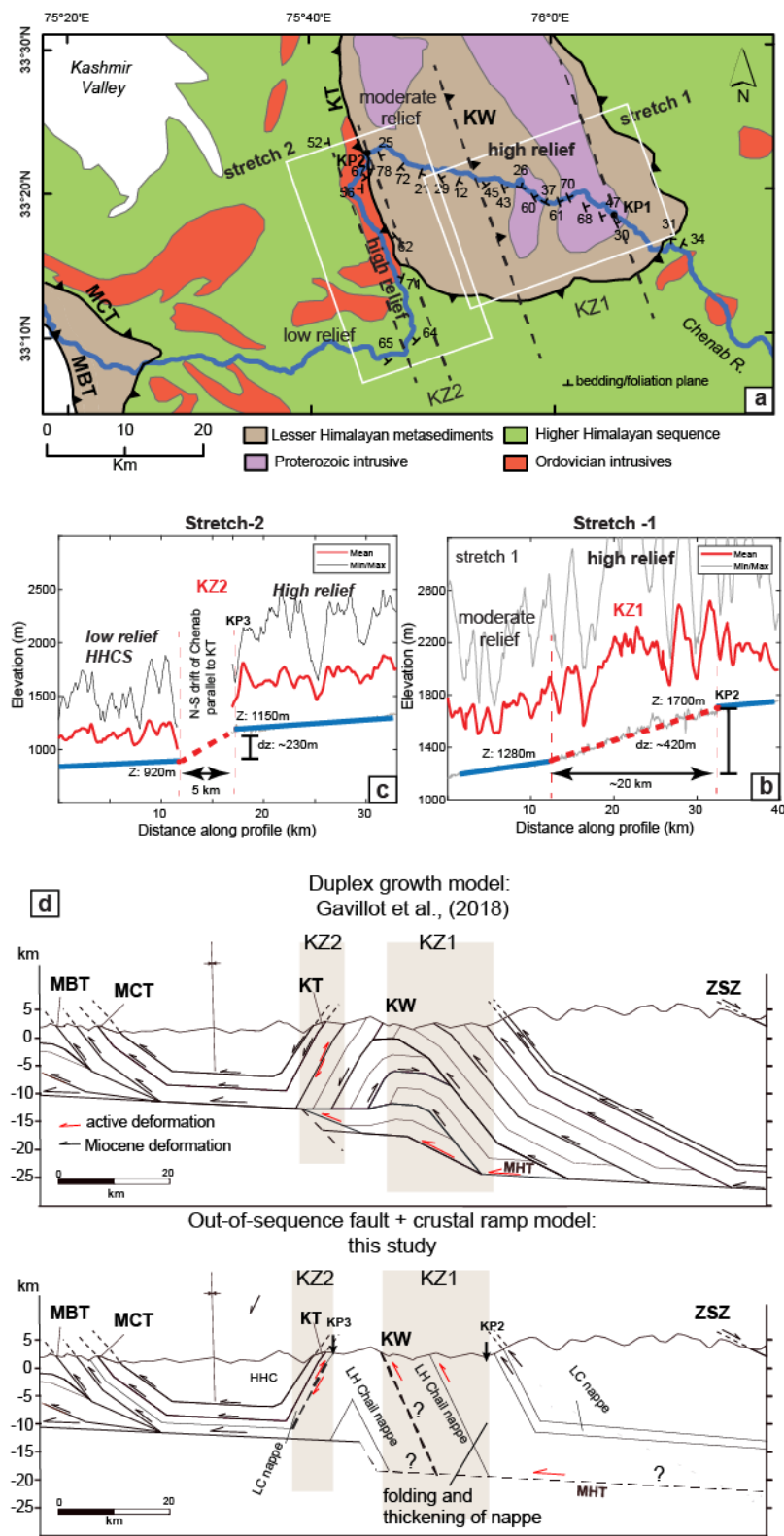
1106

Figure 7



1110

Figure 8

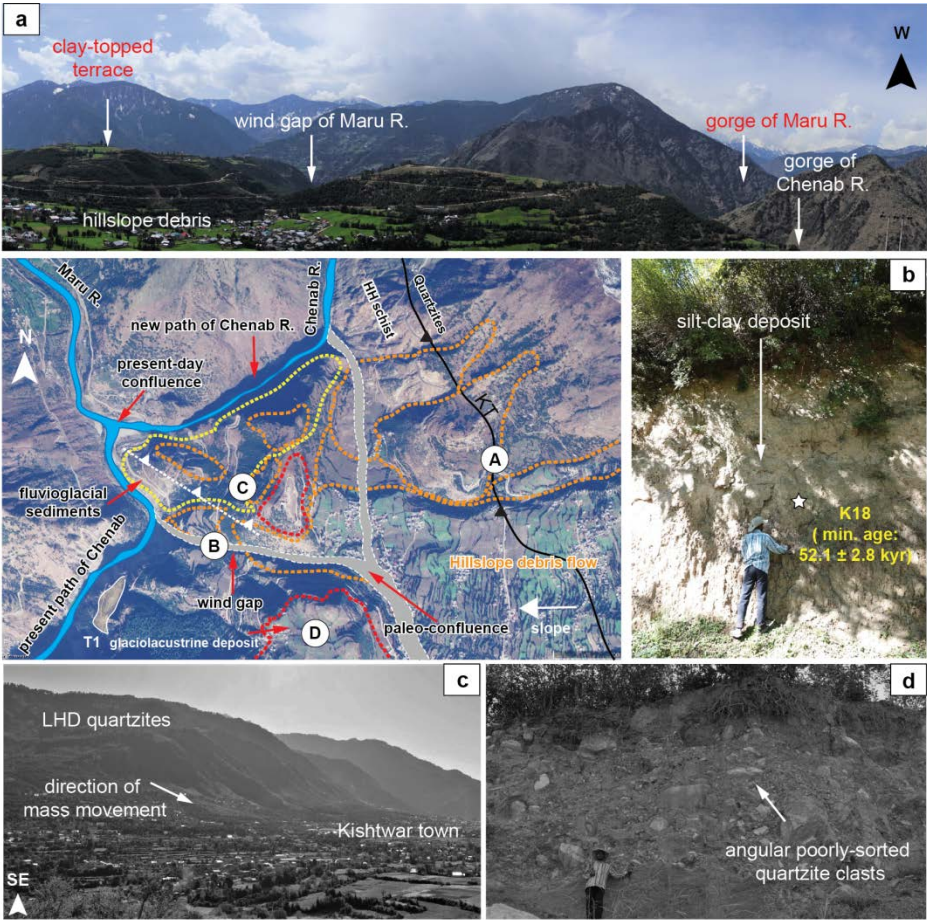


1111

1112

1113

Figure 9

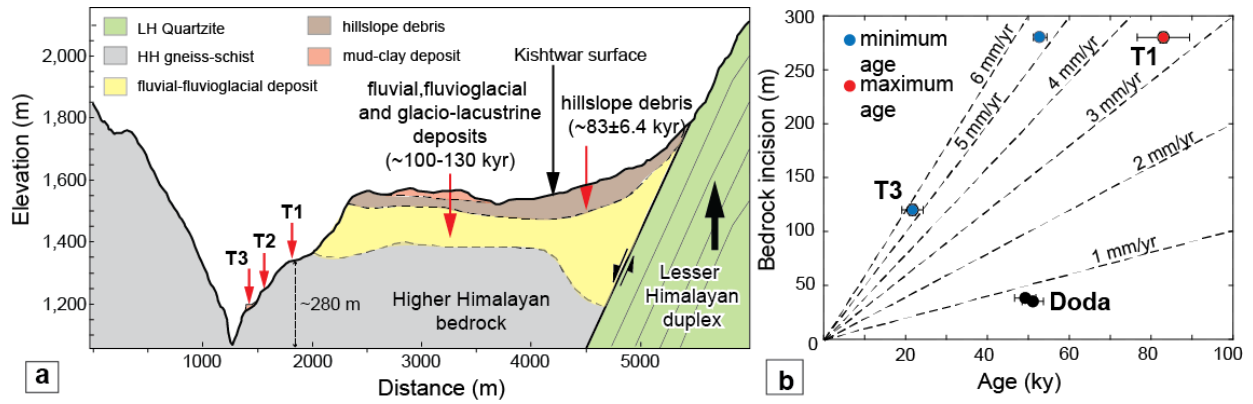


1114

1115

1116

Figure 10



1117

1118

1119

Table 1

1120

Parameter	downstream	KZ1	% change	ratio KZ1:downstream	downstream	KZ2	% change	ratio KZ2:downstream
average channel gradient (m/m)	0.006	0.021	250	3.5	0.01	0.046	360	4.6
average channel width (m)	70	45	-35.71	0.6	55	42	-24	0.76
*Specific stream power (SSP)	0.000086	0.000467	444.44	5.4	0.000182	0.001095	502	6.02

* SSP calculated by assuming equal-discharge (Q)

1121

1122

Table 2

Sample type	Sample name	Lat (°)	Long (°)	U (ppm)	Th (ppm)	K (%)	water (%)	Dose rate (Gy/ky)	De (Gy)	OD (%)	Age (ky)	fading correction	Corrected age (ky)
using central age model													
OSL	K02	33.29607	75.77619	3.8	7.2	0.46	6.1	1.74±0.02	141±8	19.5	81.1±4.6		
OSL	K11	33.35352	75.74649	3.1	12.7	2.41	6	3.97±0.09	341±19	16.8	85.7±5.1		
OSL	K01	33.15222	75.66323	2.9	13.2	2.03	9	3.88±0.04	193±11	22.1	49.8±2.9		
OSL	K06	33.15243	75.70609	3.4	18	2.17	5.4	3.97±0.05	205±10	14.4	51.6±2.4		
IRSL	K07	33.2778	75.76922	3.3	13.8	2.31	5.3	4.67±0.22	489±29	16.8	104.5±5.9	0.89	113±6
IRSL	K08	33.2778	75.76922	3.5	16.9	1.97	5.6	4.61±0.23	528±38	20.5	114.4±6.3		
IRSL	K09	33.2778	75.76922	3.3	12.2	1.98	4.8	4.29±0.20	510±42	18.1	119.2±6.8	1.11	132±7
using minimum age model													
OSL	K16	33.34873	75.73324	3.5	16.8	2.03	7.5	3.95±0.1	90±8	40	22.8±2.1		
OSL	K17	33.34873	75.73324	3.4	18	2.17	10.5	3.96±0.11	81±3.5	46	20.5±1.0		
saturated sample													
OSL	K18	33.35176	75.74325	3.3	18.7	2.61	4.5	4.36±0.13	227±14		52.1±2.8		

1123

1124

1125